# Multiscale analysis of changes in matrix structure by culturing osteoblasts

(骨芽細胞培養によるマトリックス構造変化のマルチスケール解析)

by

Yohei Hanazaki

Transdisciplinary Life Science Course, Graduate School of Life Science,
Hokkaido University

A dissertation for the degree of Ph.D.

# Table of Contents

# General introduction

## 1. Tissue engineering

Tissue engineering is an interdisciplinary field that applies the principles of engineering and life sciences toward the development of biological substitutes that restore, maintain, or improve tissue function or a whole organ [1]. The most important property required for scaffolds in tissue engineering is their ability to completely mimic native tissue structures, as tissue structure affects cell activities such as cell morphology, proliferation, and differentiation through cell-extracellular matrix (ECM) interactions [2, 3]. In this context, a combination of cells and cell scaffold is a common method of a tissue engeneered scaffold, because native tissue is mainly composed of cells and ECM. ECM is the extracellular part of animal tissue that provides structural support to the animal cells and other physiological function, and it is consisted of collagen or elastin fibers, proteoglycans, and other proteins such as fibronectin.

Therefore, various biomaterials have been developed for cell scaffold, which is usually fabricated from ECM component such as collagen. However, a scaffold with almost the same structure as that of native tissue has not been produced because mimicking the complicated anisotropic structures of native tissues has been a source of great difficulty.

Anisotropic structure of native tissue includes two featured structure; hierarchical structure and property gradient. These structures affect cell activities through cell-ECM interactions; an ideal tissue engineered scaffold must have the features.

Figure 1 is the example of native tissue structure; cartilage. Cartilage is consisted of chondrocyte and cartilage matrix. In macroscopic view, chondrocytes separately existed in cartilage matrix. More magnified view, collagen fibers and proteoglycans are observed. Collagen fibers are assembly of collagen molecules. Collagen molecule is consisted of triple-helix structure of collagen chain. This hierarchical structure (Tissue - cell - fiber - molecule - chain) is important for cartilage function and mechanical properties.

Cartilage also has a property gradient. Chan *et al* found that cartilage elastic modulus was changed from surface to deep region [4]. This change of elastic modulus made stiffness gradient, it also affect cartilage function and chondrocyte through cell-ECM interaction.

## 2. Anisotropic collagen gel scaffold (ACGS)

To mimic anisotropic structure of native tissue, anisotropic collagen scaffolds have been developed for tissue engineering so far [6-11]. For example, Lanfer *et al*. fabricated anisotropic collagen scaffold using flow deposition technique for osteoblast cultivation, and succeeded to osteoblast alignment along to the collagen orientation [6]. Lai *et al*. developed anisotropic collagen scaffold that consisted of macroscopically aligned collagen strings using straightforward flow processing technique [7]. Isobe *et al*. and Mikami *et al*. fabricated various 3D anisotropic collagen scaffolds such as mesh sheet or tube with the flow processing method, and succeeded *in vivo* transplant experiments [8, 9].

From a therapeutic stand point of view, these scaffolds are very useful. However, collagen scaffolds that have a hierarchical structure from molecule to tissue level and a properties gradient due to inhomogeneity have not been

fabricated.

Our laboratory prepared an anisotropic collagen gel by dialysis of collagen solutions into phosphate buffer solution with neutral pH values [12]. Structure of the anisotropic collagen gel scaffold (ACGS) is shown in Figure 2. The gel has a phase-separated structure. It has a high collagen concentration region (concentrated phase) and a low collagen concentration region (diluted phase), and showed birefringence (Figure 7). Diameter of the diluted phase is gradually changed about 30-200 μm from top to bottom of the gel, and it is considered to property gradient. Magnified schematic of ACGS shows that collagen fibrils were oriented circumferentially to the interface and small number of the bundle of the collagen fibrils is existed in the diluted phase. ACGS is different from isotropic collagen gel scaffolds that were prepared by a traditional method (ICGSs) at the point that ACGS has an anisotropic, hierarchy structure from molecule to macroscopic gel level and has a properties gradient. ICGS did not show birefringence which was shown by ACGS.

## 3. Osteoblast

Osteoblasts are cells that are responsible for bone formation and bone remodeling. In bone formation process, osteoblasts secrete various kinds of proteins such as Type 1 collagen to make osteoid. Osteoid is a unmineralized, organic portion of the bone matrix that forms prior to the maturation of bone tissue. Osteoid is mineralized by osteoblast. In this process, osteoblasts secret minerals into the surrounding osteoid. This process can be regarded as an elementary process of osteogenesis. However, mineral deposition into collagen matrices is unclear.

Osteoblast also play important role in bone matrix remodeling. Bone remodeling is a process where mature bone tissue is removed from the skeleton and then new bone tissue is formed. One of the important roles of bone turnover is to continuously replace and repair damaged bone tissue. Osteoblast involved both bone-resorption and bone-making processes by secreting matrixmetalloproteinase such as collagenase to remove old osteoid and making new bone tissue for secreting osteoids and minerals.

In this experiment, I use MC3T3-E1 cells. MC3T3-E1 is preosteoblastic cell line established by Sudo *et al.* [13] from newborn mouse calvaria. MC3T3-E1 easily differentiate into osteoblast using differentiation medium, and then perform bone formation.

## 4. Mechanical stimuli

Mechanical stimuli (MS) play a crucial role in the physiology of many tissues including bone. Mechanical loading can inhibit bone resorption and increase bone formation by controlling bone cells activity. MS cause deformations in bone that stretch bone cells within and lining the bone matrix and create fluid movement within the canaliculus of bone.

Bone cells are stimulated to produce second messengers when exposed to fluid flow or mechanical stretch [14-16]. In previous research, pre-osteoblastic cells were cultured in bone-mimic matrices to investigate the effect of MS on osteoblastic differentiation [17-23]. These cells were exposed to various kinds of MS modes such as shear [17-19], compressive [20, 21], and tensile forces [22, 23] *in vitro*.

In addition, MS has also profound influences on bone remodeling. Disuse or lack of loading causes an acceleration of bone turnover, with bone resorption

dominating bone formation and thus a rapid loss of bone mass. This process is responsible for imbalance of osteoblast and osteoclast activity, therefore MS application is necessary for adequate osteoblast matrix remodeling.

## 5. Small angle X-ray scattering analysis

Small-angle X-ray scattering (SAXS) technique is based on the detection of the elastic scattering of X-rays by specimens with inhomogeneities of the electron density in the nm-range. X-ray scattering in the small angle range (typically 0.1 - 10° ) contains information about the shape and size of nano-objects in dilute solution such as macromolecules, characteristic distances of partially ordered nanostructured materials, nanopore sizes, and other low resolution structure features. Typically, SAXS provides structural parameters of macromolecules with sizes between 5 and 25 nm. For dilute protein solutions, SAXS results reveal such as the oligomerization state, gyration radius, maximum diameter of proteins and conformational changes induced by ligand association, and so on.

In this study, SAXS measurements were performed at the BL40B2 beam line equipped in the SPring-8 (Japan Synchrotron Radiation Research Institute; JASRI). In this experiment system, we can observe much wider range from several angstroms to hundreds of nanometers to analyze the structures of specimens than normal SAXS equipment for laboratory use.

## 6. Aim of this study

The aim of the present study was to see how cells change and remodel the scaffolds through the cultivation of cells on matrix.

Chapter 1: Multiscale analysis of changes in an anisotropic collagen

gel structure by culturing osteoblasts

I used ACGS for the scaffold, because ACGS that has both hierarchical structure and property gradient is useful for investigating cell-ECM interactions and can be led to developing a novel scaffold for tissue engineering. As ACGS has a properties gradient, observation of a cells-ECM interaction is expected. The study on such an interaction is necessary for understanding the effect of the scaffold when used for therapeutic purpose.

## Chaper 2: Multiscale analysis of osteoblastic behavior by application of mechanical stimuli for osteoblasts.

I used collagen sponge for the scaffold. This collagen sponge is developed for MS application experiment. Therefore, I focused on MS effect for osteoblastic behavior, such as bone formation.

# Chapter 1 : Multiscale analysis of changes in an anisotropic collagen gel structure by culturing osteoblasts

## Introduction

The most important property required for scaffolds in tissue engineering is their ability to completely mimic native tissue structures, as tissue structure affects cell activities such as cell morphology, proliferation, and differentiation through cell-extracellular matrix (ECM) interactions [1, 2]. In this context, various kinds of scaffolds have been developed so far. However, a scaffold with almost the same structure as that of native tissue has not been produced because mimicking the complicated anisotropic structures of native tissues has been a source of great difficulty.

Furthermore, native tissue has properties gradually changing in space, resulting in a gradient of the properties, such as stiffness gradient [4]. Biomaterials helping a tissue generation often have properties or structural gradient [5]. It is expected that such a properties gradient derived from inhomogeneous structures of native tissue could help cells to perform remodeling of the tissue through cell-ECM interactions.

To mimic anisotropic structure of native tissue, anisotropic collagen scaffolds have been developed for tissue engineering so far [6-11]. For example, Lanfer *et al*. fabricated anisotropic collagen scaffold using flow deposition technique for osteoblast cultivation, and succeeded to osteoblast alignment

along to the collagen orientation [6]. Lai *et al*. developed anisotropic collagen scaffold that consisted of macroscopically aligned collagen strings using straightforward flow processing technique [7]. Isobe *et al*. and Mikami *et al.* fabricated various 3D anisotropic collagen scaffolds such as mesh sheet or tube with the flow processing method, and succeeded *in vivo* transplant experiments [8, 9].

From a therapeutic stand point of view, these scaffolds are very useful. However, collagen scaffolds that have a hierarchical structure from molecule to tissue level and a properties gradient due to inhomogeneity have not been fabricated. The anisotropic scaffold that has both hierarchical structure and property gradient is useful for investigating cell-ECM interactions and can be led to developing a novel scaffold for tissue engineering.

Furusawa *et al*. prepared an anisotropic collagen gel by dialysis of collagen solutions into phosphate buffer solution with neutral pH values [12]. They confirmed that the anisotropic collagen gel (ACGS) had a hierarchical structure and a properties gradient [12]. Generally, interaction of cells with their matrix has been known to change with the change in matrix properties. When cells are cultured on a matrix having a properties gradient, the interaction would be highlighted. As ACGS has a properties gradient, observation of a cells-ECM interaction is expected. The study on such an interaction is necessary for understanding the effect of the scaffold when used for therapeutic purpose. The aim of the present study was to see how cells remodel the scaffolds as the result of a cell-ECM interaction through the cultivation of cells on ACGS. For this propose, I cultured osteoblastic cells on ACGS, which I regarded as a model system for the cell-ECM

interaction. Changes in the ACGS-cell composites structure by remodeling was investigated from a macroscopic to microscopic level. The cultured cell-gel composite was investigated macroscopically by confocal laser scanning microscopy and microscopically by small-angle X-ray scattering (SAXS). The results were discussed how cells adopt ACGSs based on the morphology observation.

Structure of the anisotropic collagen gel scaffold (ACGS) is shown in Figure 2. The gel has a phase-separated structure. It has a high collagen concentration region (concentrated phase) and a low collagen concentration region (diluted phase), and showed birefringence (Figure 7). Diameter of the diluted phase is gradually changed about 30-200 μm from top to bottom of the gel, and such a structure is relating to a property gradient. Magnified schematic picture of ACGS shows that collagen fibrils were oriented circumferentially to the interface and small number of the bundle of the collagen fibrils is existed in the diluted phase. ACGS is different from isotropic collagen gel scaffolds that were prepared by a traditional method (ICGSs) at the point that ACGS has an anisotropic, hierarchy structure from molecule to macroscopic gel level and has a properties gradient. ICGS did not show birefringence as observed in ACGS (Figure 7).

I used osteoblastic MC3T3-E1 cell line as the testing cells because they are one of the most studied cells. Residing in bone tissue, osteoblasts are responsible for bone mineralization by the secretion of calcium phosphates and for the remodeling of bone. In the latter process, osteoblasts secrete collagenase to digest collagen and reconstruct collagen matrix[24]. Mechanical stimuli (MS) have long been regarded to play an important role in osteoblast

differentiation [14-16]. In previous research, pre-osteoblastic cells were cultured in bone-mimic matrices to investigate the effect of MS on osteoblastic differentiation [17-23, 25, 26]. Therefore, I applied MS to ACGS-osteoblast composite.

# Materials & Methods

## 1. Solution preparation

I used an “atelo-collagen” for this study, which was purchased in 5 mg/mL 1 mM HCl aqueous solution at pH 3.0 from Koken Co. Ltd. (Tokyo, Japan). A phosphate buffer solution (PBS) consisting of $KH_2PO_4$ and $Na_2HPO_4$ (Wako Pure Chemical Co. Ltd, Osaka, Japan) was prepared. Concentrations of $KH_2PO_4$ and $Na_2HPO_4$ were 13 mM and 20 mM, respectively. The pH of PBS was 7.0 at 30 ℃ .

The growth medium was Minimum Essential Medium Alpha (MEM $\alpha$ , Wako) supplemented with 10% FBS (fetal bovine serum; PAA Laboratories, Austria) and 1% penicillin–streptomycin (Sigma Chemicals, Missouri, USA). The differential medium was the growth medium supplemented with 2 mM glycerophosphate disodium salt pentahydrate (MP Biomedicals, California, USA) and 50 $\mu$g/ml L-ascorbic acid phosphate magnesium salt n-hydrate (Wako).

## 2. ACGS and ICGS preparation

Figure 3 shows the schematic illustration of a dialysis chamber (10 mm in diameter, 3 mm in thicknesses) to prepare collagen gel scaffolds. The collagen solution chamber consists of two silicon rubber sheets with a thickness of 1.5 mm set on a 35mm cell culture plastic dish (Thermo scientific, Massachusetts, USA). The collagen solution (150 μl) was injected into the chamber. A dialysis membrane was set on the top of the collagen solution chamber, and a silicon rubber well was then put on the dialysis membrane. To prepare ACGS, PBS was poured over the silicon rubber well.

Conversely, the growth medium was poured over the silicon rubber well to prepare ICGS. During the dialysis process of the collagen solution into PBS or the growth medium, the collagen gel phase grew from the dialysis membrane from the top to the bottom of the chamber. Scaffolds were incubated for 2 hours at 30 ℃. After removing PBS and the dialysis membrane, scaffolds were immersed in the growth medium and incubated overnight in a 37 ℃, 5 % $CO_2$ incubator. For application of MS, the upper silicon rubber sheet was removed before cell seeding on scaffolds. To observe the macroscopic morphology of ACGS and ICGS, I took optical images using a DMC-GF2 digital camera (Panasonic Corporation, Osaka, Japan) and NANOHA x5 ultra-macro lenses (Yasuhara Co. Ltd., Nagoya, Japan) under natural light, polarized light, and circular polarized light.

For investigating effect of gelling temperature on ACGS structure, thin ACGS films were fabricated (Figure 19). Thin ACGS films were prepared by a following procedure. 200 mL of collagen solution was put on a 100 mm dish, and then a circular cover glass with a diameter of 18 mm was put on the collagen solution. To prepare the thin ACGS film, 20 mL of PBS was poured into the dish. To investigate the effect of temperature on macroscopic morphology of ACGS, the thin ACGS films were prepared at 10 ℃, 20 ℃, and 30 ℃.

To evaluate the functional ability of ACGS for bone-tissue engineering, another thin ACGS film and ICGS film for control were fabricated for MC3T3-E1 cells cultivation. These film were prepared by a following procedure (Figure 20A). 80 mL of collagen solution was put on a 35 mm dish, and then a circular cover glass 12 mm in diameter was put on the

collagen solution. To prepare the thin ACGS film, PBS was poured into the 35 mm dish. On the other hand, the growth medium was poured into the 35 mm dish to prepare the thin ICGS film. The thin ACGS film has a spoke like (radially extending) pattern consisted of the concentrated phase and the diluted phase (Figure 20B).

## 3. Cell culture

The osteoblastic cell line (MC3T3-E1 cells) was provided by RIKEN BRC through the National Bio-Resource Project of MEXT, Japan. MC3T3-E1 cells were cultured in the growth medium. Cells were cultured on a cell culture plastic dish (FG-2090; Nippon Genetics Co. Ltd, Tokyo, Japan) in an incubator regulated at 37℃ and 5% $CO_2$. Cells at passage 5 were seeded on ACGS (MC3T3-E1/ACGS composite) and ICGS (MC3T3-E1/ICGS composite). Seeding density was $3.0 \times 10^4$ cells/gel. Two days after seeding, the medium was changed to the differentiation medium. The medium was changed every 3 days. Specimens were taken from a dish at day 7, day 14, and day 21, and were used in the following experiments.

For application of ACGS for osteoblast cultivation, I investigated the calcification behavior induced by MC3T3-E1 cells on the ACGS (Figure 20). To remove the cover glass from the thin ACGS film, PBS was exchanged with the growth medium. Then, the scaffolds were incubated at 37 ℃ for overnight. After the incubation, the cover glass can be easily removed from the surface of the scaffolds. MC3T3-E1 cells were seeded on the surface of the scaffolds at the seeding density of $2.2 \times 10^3$ cells/$cm^2$. The specimens were incubated in the growth medium for 3 days, and then the growth medium was exchanged with the differentiation medium that is the growth medium

supplemented with 2 mM b-glycerophosphate disodium salt pentahydrate and 50 $\mu$g/ml L-ascorbic acid phosphate magnesium salt n-hydrate. Medium was changed every 3 days. The specimens were taken from a dish at day 10 and 21.

## 4. MS application

MS was applied to MC3T3-E1 cells using the MS-application apparatus shown in Figure 4. The device monitors compressive deformation by a deformation sensor in real-time. The device was placed in the 37 ℃ , 5% $CO_2$ incubator. The specimen was set on the stage. A cyclic compressive strain was directly applied to specimens by an aluminum indenter (10 mm in thickness, 30 mm in diameter, cylindrical shape). Strain amplitude and the frequency of MS were controlled at 3000 $\mu\varepsilon$ and 3 Hz, respectively (Figure 5). MS was applied for 1 h per day from day 0 to day 6.

## 5. Conforcal laser scanning microscope observation

To observe the morphology of specimens, collagen molecules, actin fibers, and nuclei were visualized using immunofluorescence staining for collagen molecules, Alexa Fluor 488-conjugated phalloidin for actin fibers, and SYTOX® Blue for nuclei, respectively.

A blocking solution, primary antibody solution, and secondary antibody solution were prepared. The blocking solution consisted of 10% FBS and 0.5% Triton X-100 (Wako) in phosphate buffer saline consisting of 2.3 mM of KCl, 1.5 mM of $KH_2PO_4$, 8.4 mM of $Na_2HPO_4$ and 137 mM of NaCl at pH 7.4 (PBS(-)). An anti-collagen alpha I (SC-8784-R, Santa Cruz Biotechnology, Inc., California) diluted 1:200 in the blocking solution was used as the primary

antibody solution. An Alexa Fluor 633-conjugated anti-rabbit IgG (Molecular Probes, Life Technologies Corporation, California, USA) diluted 1:1000 in the blocking solution was used as the secondary antibody solution. 300 units of Alexa Fluor 488-conjugated phalloidin (Molecular Probes) solution was diluted 1:60 in PBS(-). 5 mM of SYTOX® Blue solution (Molecular Probes) was diluted 1:5000 in PBS(-).

Collagen staining: Specimens were washed with PBS(-) three times, then fixed by 4% formaldehyde for 30 min at 4℃. Specimens were blocked and permeated with blocking solution at room temperature for 3 h. Specimens were then incubated with the primary antibody solution overnight at room temperature. Specimens were washed three times with PBS(-), followed by incubation at room temperature for 3 h in the secondary antibody solution.

Actin fiber staining: Specimens were washed three times with PBS(-), and were then treated with phalloidin solution for 3 h.

Cell nucleus staining: Specimens were stained with SYTOX® Blue solution for 1 h.

Specimens were mounted on a coverslip and observed by a confocal laser scanning microscope (CLSM; Leica TCS SP5).

I took a surface region image (from the gel surface to 30 μm deep) and an inner region image (from 30 μm to 60 μm deep) for each specimen. I counted cell numbers in 450 × 450 μm area at each regions .

## 6. SAXS measurements

SAXS measurements were performed at the BL40B2 beam line equipped in the SPring-8 (Japan Synchrotron Radiation Research Institute; JASRI). The

X-ray wavelength was 1.5 Å. The incident X-ray beam was parallel to the growth direction of the collagen gel layer (Figure 6). Sample-to-detector distance was 4250 mm. SAXS patterns were acquired with a CCD camera (C4880, Hamamatsu Photonics, Japan) with an X-ray imaging intensifier (IV4554P, Hamamatsu Photonics). Exposure times were 5 s or 10 s. I selected the proper exposure time for each specimen to prevent a saturating scattering intensity. All experiments were performed at 37 ℃ . 2D SAXS patterns were corrected by subtracting the dark current of the detector. To obtain 1D SAXS profiles, the circular average of 2D SAXS patterns were calculated. The averaged scattering intensity I(q) was plotted as a function of scattering vector q, defined as $q = (4\pi / \lambda)\sin(2\theta/2)$, where $2\theta$ is the scattering angle.

## 7. WAXD measurements

The WAXD measurement was performed at the BL40B2 of the SPring-8. The wave length of X-ray was 0.8 Å. The 2D WAXD pattern was acquired using the CMOS flat panel 2D image sensor (C9728DK-10, Hamamatsu Photonics). The sample-to-detector distance was 62 mm. The 1D WAXD profiles were obtained by circular averaging the 2D WAXD patterns (Figure 20).

## 8. Statistical analysis

All experiments were performed three times. Statistical differences were assessed with a one-way ANOVA. Calculations were performed by SigmaPlot (version 11.0, Hulinks Inc., Tokyo, Japan).

# Results & Discussion

## 1. Macroscopic morphology of ACGS and ICGS

I observed macroscopic morphology to confirm difference between ACGS and ICGS structure. Figure 7A shows the macroscopic morphology of ACGS under natural light. A turbid network and transparent pores were observed. In previous research, Furusawa *et al.* found that the turbid network was the high collagen concentration region (concentrated phase) and transparent pores were the low collagen concentration region (diluted phase) [12]. On the other hand, no apparent macroscopic morphology was observed in ICGS (Figure 7B).

Images of ACGS and ICGS under polarized light are shown in Figure 7C and D, respectively. In Figure 7C, the concentrated phase of ACGS showed birefringence. This pattern suggested that collagen fibrils were oriented either radially or circumferentially to the interface between the concentrated and the diluted phases. In contrast, ICGS did not show birefringence (Figure 7D).

To determine the orientation of collagen fibrils, ACGS was observed under circular polarized light (Figure 7E). In this experiment, a pair of circular polarizers and quarter-wave plates was arranged as previously described by Maki *et al*. [27]. In this arrangement, if the collagen fibril is oriented parallel to the slow axis of quarter-wave plates, it will show a blue color under natural light. On the other hand, if the collagen fibril is oriented perpendicular to the slow axis of quarter-wave plates, it will show an orange color under natural light. The interface between the diluted phase and concentrated phase of ACGS showed blue and orange colored sectors as shown in Figure 7E. This

result suggests that collagen fibrils align parallel to the interface in the plane parallel to the gel surface, which is consistent with the results of CLSM images of ACGS in previous research [12]. On the other hand, ICGS did not show birefringence. These results confirm that ACGS has an anisotropic structure and ICGS has an isotropic structure.

## 2. Confocal Laser Scanning Microscope observation

Low-magnified CLSM images of MC3T3-E1 cells/ACGS (anisotropic gel) composites (ACGS-MS-), MC3T3-E1 cells/ICGS (isotropic gel) composites (ICGS-MS-), mechanically stimulated MC3T3-E1 cells/ACGS composites (ACGS-MS+), and mechanically stimulated MC3T3-E1 cells/ICGS composites (ICGS-MS+) at 7 days, 14 days, and 21 days cultivation were shown in Figure 8, 9, and 10, respectively. Osteoblasts existed uniformly and densely in surface regions. Significant differences in cell distribution on the surface region were not observed among all specimens and all cultivation time. This result suggests that ACGS has as good a cell attachment and biocompatibility as ICGS.

In the inner region of ACGS, small number of osteoblastic cells were found only in the diluted phase (Figure 8A, B) in 7 days cultivation specimens. However, osteoblastic cells were observed randomly in the inner region of ICGS (Figure 8C, D). In 14days specimens, more osteoblastic cells were existed in the diluted phase in ACGS (Figure 9A, B). In contrast, osteoblastic cells were observed individually and randomly in the inner region of ICGS (Figure 9C, D). Same cell distribution was observed in 21 days cultivation; cell number was not increased compared to 14days (Figure 10).

In ACGS, the elasticity of the matrix is different in the diluted phase and

concentrated phase, and the interface between the two phases has the highest elasticity difference. As reported in the literature, osteoblasts prefer migrating on the stiffer matrix [28-30]. In ACGS, collagen molecular density in concentrated phase $\rho_C$ is larger than those of ICGS, $\rho_{ICGS}$. The density of the diluted phase in ACGS($\rho_D$) is smaller than that of ICGS ($\rho_C > \rho_{ICGS} > \rho_D$). This means the order of modulus in each phase should be $E_C > E_{ICGS} > E_D$ (C, ICGS, and D indicate the same meaning as those in $\rho$). Cells in ICGS might migrate by developing the space through protease digestion. The permeation of cells would be the easiest in the diluted phase of ACGS. Therefore, osteoblastic cells would migrate into ACGS by attaching on the interfacial walls between dilute and concentrated phases in ACGS.

The magnified image of the shallow or deep part of ACGS-MS- specimen at 14 days cultivation was shown in Figure 11A and B, respectively. In the shallow part of diluted phase of ACGS, osteoblastic cells seemed to pull and collect collagen fibrils from the concentrated phase (Figure 11A). This result suggests that collagen fibrils in the diluted phase of ACGS would be modified by the cells. In the deep region of ACGS, where the diameter of the diluted phase increased, the cells constructed a toroidal structure along with the wall of the diluted phase, and relatively concentrated collagen fibrils were observed in the center of the diluted phase (Figure 11B).

These results indicate that osteoblastic cells attach on the interface between the diluted and concentrated phases and that they increase the concentration of collagen fibrils at the center of the diluted phase. With the change in diameter of diluted phase, morphology of cell in the diluted phase changed. Altogether, cell-matrix interaction and cell morphology varied along

with the variation in anisotropic structure of ACGS.

A schematic diagram of osteoblastic cell invasion into ACGS is shown in Figure 12. At first, the cells proliferated on the ACGS surface to become confluent. Then, they started invading into the inner region (Figure 12A). Osteoblastic cells collected the collagen fibrils in the diluted phase at the shallow region (Figure 12B). However, in the deep region, as the diameter of the dilute phase increased, the cells would attach on the interface between the concentrated and diluted phases to construct a toroidally aggregating structure, and collect collagen fibrils to the center of the diluted phase (Figure 12C).

In the top layer of ACGS, collagen fibrils would distribute randomly as in ICGS. Significant differences in cell behavior in ACGS from that in ICGS were observed only in the inner regions. In ICGS specimens, the number of the cells inside ICGS seemed to increase with MS application. In ACGS specimens, the morphology or orientation of osteoblasts in surface regions were similar to that of ICGS.

As for the shape of cells in ACGS and ICGS, according to the magnified images, each of cells in all the images is essentially in the spindle shape, though aggregates of cells look dendritic. However, there are cells in ACGS look slightly different from those in ICGS. For the understanding of this difference, information should be needed after further investigation.

## 3. Cell invasion assay

To analyze the invasion ability of osteoblastic cells to matrix quantitatively, I counted the number of the cells distributed in surface and inner regions

(Figure 13). The ratio of the number of cells existing in the inner region to the total cell number is expressed as

$$\frac{N_i}{N_i+N_s} \quad (1)$$

where $N_i$ and $N_s$ are the number of cells existing in the inner and surface regions, respectively. In all specimens, almost all cells existed in surface regions and only several cells were found in inner regions at 7 days cultivation, where the number of cells was larger for ACGS than ICGS. At 14 days cultivation, significant increases in cells staying in the inner regions were observed in all specimens. About 30% of cells invaded into the inner regions in ACGS, while only 20% of cells existed in the inner regions in ICGS. In 21 day culture specimens, however no significant increases in cell numbers in the inner regions were observed in all specimens. Cell invasion seems to have been saturated after 14 days. In ICGS specimens, MS seems to promote the significant invasion of osteoblasts to the matrix at days 7 and 14 as in other reports [31-33]. However, such a change by MS was not observed in ACGS specimens. These results indicate that the MS effect on the invasion ability of osteoblastic cells is much smaller than that of the ACGS anisotropic structure.

## 4. Small-angle X-ray scattering analysis

2D SAXS patterns for ACGS, ICGS, ACGS-MS-, ACGS-MS+, ICGS-MS-, and ICGS-MS+ are shown in Figure 14. An isotropic scattering pattern was observed in all specimens. Although ACGS has an anisotropic structure, no anisotropy was observed in 2D SAXS patterns for ACGS. Furusawa *et al.* previously showed that the orientation of collagen fibrils in the cross-sectional plane perpendicular to the growth direction of anisotropic collagen

gel is the circumferential direction generally parallel to the interface [12]. Therefore, the isotropic 2D SAXS pattern for ACGS can be attributed to such a planer orientation of collagen fibrils as described above.

## 4-1. Scattering from ACGS and ICGS

Log-log plots of SAXS profiles for ACGS and the ICGS are shown in Figure 15A. At the low-q region (0.02 $nm^{-1}$ < q < 0.04 $nm^{-1}$), the logarithm of I(q) for ACGS linearly decreased with an increasing logarithm of q. At the high-q region (q > 0.04 $nm^{-1}$), logarithms of I(q) for ACGS also decreased linearly with increasing of the logarithm of q but with a steeper slope. Therefore, SAXS profiles I(q) for ACGS can be regarded to consist of two power-law regions, a $_{low\text{-}q}$ region and a $_{high\text{-}q}$ region. The power law relationship between I(q) and q can be expressed as

$$I(q) \propto q^{-a} \qquad (2)$$

where a is the scattering exponent of the power-law. Scattering exponents were calculated from the slopes of linear regions in the log-log plot. The scattering exponent at the low-q region, $a_{low\text{-}q}$, for ACGS ($a_{low\text{-}q}$ = 2.07 $\pm$ 0.04) was smaller than that at the high-q region, $a_{high\text{-}q}$, for ACGS ($a_{high\text{-}q}$ = 3.53 $\pm$ 0.11). Scattering exponents have been reported to be related to the fractal dimensions of the structure of scattering bodies [34]. The $a_{low\text{-}q}$ is attributed to a mass fractal dimension ($D_m$). The mass fractal dimension has a value from 1 to 3, and is related to the compactness of the scattering bodies packing. The relationship between the $a_{low\text{-}q}$ and $D_m$ is expressed as

$$D_m = a_{low\text{-}q} \qquad (3)$$

Small values of $D_m$ indicate looser structures and large values of $D_m$

indicate compact structures. On the other hand, $a_{high\text{-}q}$ is related to a surface fractal dimension ($D_s$). The surface fractal dimension has a value of 2 to 3, and relates to the roughness of the surface of the scattering bodies. The relationship between the $a_{high\text{-}q}$ and $D_s$ is expressed as

$$D_s = 2D - a_{high\text{-}q} \qquad (4)$$

where D is the dimension of the scattering bodies. For 3-dimensional scattering bodies, D = 3. If $D_s$ is small, the surface of the scattering bodies is smooth. On the other hand, if $D_s$ is large, the surface of the scattering bodies is rough.

No linear region was observed at the low-q region in the log-log plot for ICGS. On the other hand, the logarithm of I(q) at the high-q region in the log-log plot for ICGS linearly decreased with an increasing logarithm of q. There was no significant difference between $a_{high\text{-}q}$ values for ACGS and for ICGS.

Consequently, in the low-q region, the linear region was observed only in ACGS. However, in the high q region, the linear relation in I(q) vs. q was observed in both ACGS and ICGS. There was no significant difference between $a_{high\text{-}q}$ values for ACGS and for ICGS.

## 4-2. Scattering from cell-seeded AGCS

Log-log plots of SAXS profiles for cell-seeded scaffolds were shown in Figure 15B-E. In all specimens, the scattering intensity was increased by cell-seeding, though the increment did not change in the order of the culturing period. During cell culturing, decrease in the volume of the scaffold was observed, resulting in an increase in concentration of collagen fibrils in the scaffolds. The increase in scattering intensity can be attributed to these

changes in the scaffolds. A weak scattering maximum was observed near $q_m$ = 0.093 $nm^{-1}$ in all specimens. Spacing corresponding to the $q_m$ calculated from Bragg's law was 67.5 nm. As the value was nearly equal to the D-period of collagen fibrils, results suggest that the scattering behavior is mainly due to collagen fibrils and/or aggregates of collagen fibrils.

To discuss changes in the higher order structure of collagen fibrils in cell-seeded specimens, scattering behavior in the q range from 0.018 $nm^{-1}$ to $q_m$ were further analyzed. Scattering curves from ACGS-MS- and ACGS-MS+ have two power-law regions: the low-q region (0.018 $nm^{-1}$ < q < 0.04 $nm^{-1}$) and high-q region (0.04 $nm^{-1}$ < q < 0.08 $nm^{-1}$) (Figure 15B, C). I calculated $a_{low\text{-}q}$ and $a_{high\text{-}q}$ from the slope of the straight lines in log-log plots for ACGS-MS- and ACGS-MS+. Changes in $a_{low\text{-}q}$ and $a_{high\text{-}q}$ along with the cultivation time are shown in Figure 16A, B. At day 7, values of $a_{low\text{-}q}$ for ACGS increased from 2.07 $\pm$ 0.04 to 2.95 $\pm$ 0.02 for ACGS-MS- and to 3.02 $\pm$ 0.03 for ACGS-MS+ by cell-seeding. After day 7, $a_{low\text{-}q}$ decreased with increases in the cultivation time. Values of $a_{low\text{-}q}$ were in the range of 1 to 3, indicating the mass fractal dimension. The increase in $a_{low\text{-}q}$ due to cell-seeding indicates that scattering bodies are packed more compactly. The decrease in $a_{low\text{-}q}$ after day 7 of culture suggests that the packing of the scattering bodies becomes loose with increases in the cultivation time. There were no significant changes in the values of $a_{high\text{-}q}$ during cell culturing, irrespective of cultivation conditions (Figure 16B). Since the values of $a_{high\text{-}q}$ were in the range of 3 to 4, the values of $a_{high\text{-}q}$ are related to the surface fractal dimension. This result demonstrates that the roughness of the bodies in ACGS-MS- and ACGS-MS+ does not change during the cell culture. No significant effects of mechanical stress on changes

in both $a_{low\text{-}q}$ and $a_{high\text{-}q}$ were observed.

## 4-3. Scattering from cell-seeded ICGS

For both ICGS-MS- and ICGS-MS+, two linear regions were observed at the low-q region (0.018 $nm^{-1}$ < q < 0.03 $nm^{-1}$) and high-q region (0.05 $nm^{-1}$ < q < 0.08 $nm^{-1}$) in log-log plots, respectively (Figure 15D, E). Values of $a_{low\text{-}q}$ for ICGS-MS- and ICGS-MS+ increased with increases in the cultivation time. Values of $a_{low\text{-}q}$ for ICGS-MS- and ICGS-MS+ were in the range of 1 to 3, indicating the mass fractal dimension. Therefore, the increase in the $a_{low\text{-}q}$ for ICGS-MS- and ICGS-MS+ suggests that the packing of the scattering bodies becomes tight with the cell culture. There were no significant changes in the values of $a_{high\text{-}q}$ during the cell culture, irrespective of cultivation conditions (Figure 16B). Since the values of $a_{high\text{-}q}$ were in the range of 3 to 4, the values related to the surface fractal dimension. This result indicates that the roughness of the surface of scattering bodies in ICGS-MS- and ICGS-MS+ does not change during the cell culture. No significant effects of mechanical stress on changes in the $a_{low\text{-}q}$ were observed.

## 4-4. Size of scattering bodies

To determine characteristic sizes of scattering bodies in specimens, the scattering intensity in the q range between 0.018 $nm^{-1}$ and 0.08 $nm^{-1}$ was analyzed by the modified Guinier analysis [35]. The collagen fibril can be regarded as a rod-like particle with the contour length L, cross-sectional area A, and radius of the cross-section $R_c$. For the q range between 1/L and $1/r_c$, the scattering intensity of the rod-like particle is approximately expressed as

$$I(q) \approx \frac{\pi A^2 \Delta\rho}{qL} e^{-\frac{r_c^2 q^2}{2}} \qquad (5)$$

where $\Delta\rho$ is the electron density difference between rod-like particles and solvent, and $r_c$ is the radius of the gyration of the cross-section of rod-like particles. For the circular cross-section, $R_c = r_c / \sqrt{2}$. The values of $r_c$ were calculated from the slopes of the straight lines in cross-section Guinier plots (lnqI(q) vs. $q^2$). Cross-section Guinier plots for ACGS and ICGS were shown in Figure 17A. Two linear regions were observed in cross-section Guinier plots for both scaffolds. Shapes of cross-section Guinier plots suggest the polydispersity of rc of the rod-like particles. Therefore, ACGS and ICGS consisted of rod-like particles with various diameters. From an initial slope of the cross-section Guinier plot, I calculated a radius of the cross-section for thick rod-like particles ($R_{c,l}$). On the other hand, a radius of the cross-section for thin rod-like particles ($R_{c,s}$) was calculated from the slope of the linear region observed in the high-q region of the cross-section Guinier plot. The $R_{c,l}$ for ACGS was larger than that for ICGS, whereas $R_{c,s}$ for ACGS was approximately equal to that for ICGS, as shown in Figure 18A and B, respectively. $R_{c,s}$ for ACGS and ICGS were nearly equal to the radius of a single collagen fibril reported in the literature [36]. Thus, the $R_{c,s}$ would be the radius of a single collagen fibril. On the other hand, in the literature, it was also reported that bundles of collagen fibrils were formed in the collagen hydrogel prepared from the acid-soluble collagen [37]. The $R_{c,l}$ for ACGS and ICGS were comparable with radii of the bundles of collagen fibrils reported in the literature. Therefore, the $R_{c,l}$ could correspond to the radius of the bundles of collagen fibrils.

$R_{c,l}$ for ACGS-MS- and ACGS-MS+ increased with cell seeding, and then decreased with increases in the culture time. On the other hand, $R_{c,l}$ for ICGS-MS- and ICGS-MS+ increased with cell seeding, and then increased with increases in the culture time. In all specimens, no significant changes in $R_{c,s}$ were observed. The results suggest that the remodeling process of bundles of collagen fibrils is dependent on the scaffold structure, whereas that of the collagen fibril itself is independent on the scaffold structure. No significant effect of the mechanical force on changes in $R_{c,l}$ and $R_{c,s}$ was observed.

## 5. Relationship between macroscopic and microscopic observations in ACGS

In the macroscopic observation, collagen fibrils were modified by osteoblastic cells in ACGS (Figure 11A). In the microscopic observation, the packing and bundle diameter of collagen fibrils were changed both in ACGS and ICGS (Figure 16, 18), and remodeling process of the collagen bundles in ACGS was different from that in ICGS (Figure 18). These results indicate that the bundles of collagen fibrils are reconstructed by osteoblastic cells. In this experimental system, there would be two species of collagen molecules; 1) matrix collagen molecules originated from bovine atelo-collagen, and 2) osteoblastic cell-secreted collagen molecules. As mentioned above, the diameter of collagen fibrils was reported to be about 50 nm [36]. The diameter of collagen fibers produced by osteoblastic cells was reported to be 30-45 nm in 8-12 days culture [38]. Therefore, we cannot determine the origin of the collagen fibrils obtained here from the diameter. The diameter of collagen fibrils was changed after seeding of osteoblastic cells; thus, collagen fibrils appear to be modified by osteoblastic cells. Collagen fibrils were collected

in the diluted phase in ACGS. These collagen fibrils seemed to be the matrix collagen because osteoblasts may not produce such thick fibrils.

These results suggest that osteoblastic cells change the diameter of collagen fibrils and both cell- and matrix-derived collagen fibrils are modified by the cells both in ACGS and ICGS. Remodeling of collagen fibrils would be affected by the difference of the scaffold structure.

## 6. The effect of MS for osteoblastic behaviors

Mechanical stimulation (MS) has long been revealed as crucial for osteogenesis. Osteogenesis can be regarded as one of phenotypes of osteoblastic cells-ECM interaction. In my results on MC3T3-E1 osteoblastic cell and ECM interaction, however, the effect of MS was not clearly observed in ACGS specimens, while MS significantly increased osteoblastic cells invasion into ICGS matrix. Explanation for the ineffectiveness of MS on the osteogenensis in my case could be (1) that MS applied here was not optimum. Strain and frequency of applied MS is 3000 μ$\varepsilon$ and 3 Hz, these parameters mimic MS exposed to bone *in vivo* [15]. Many studies also applied such a high strain and low frequency MS for osteoblastic cells [20-22, 24]. Contrary to this, there are reports that low strain and high frequency is more effective for osteoblastic differentiaion in previous reports [39, 40]. Furthermore, Dumas *et al*. used combination of high strain and low frequency and high low strain and high frequency MS, and this dual frequency cyclic strain was enhanced osteoblast differentiation [41]. Other possibility is a period and timing of MS application. Some response to MS such as an intracellular $Ca^{2+}$ increase is a fast process; MS effects diminish just after MS application. However, Kreke *et al*. reported that osteoblastic gene was up-regulated 13 days after

MS application was stopped [42]. Optimization of MS application would be needed to enhancement on matrix remodeling activity of osteoblastic cells. The second explanation would be (2) that changes in ECM by MS locate far downstream the events of immediate response to MS such as gene or protein expressions. There is a possibility that the change in ECM would not be detected even though gene or protein expressions were observed.

However, both of these do not present a convincing explanation for the selective effect of MS on ICGS. The plausible explanation for my results may be that the MS applied in the experiments was not an optimum one for ACGS, though the MS parameters have been said to be normal in animals' life. However, it is also a fact that a MS applied to a scaffold is not necessary optimum to scaffolds having different structures and mechanical properties. Further biological study is needed to fully understand the effect of MS application on osteoblastic behavior, though it is beyond the scope of the present study.

## 7. Effect of diluted phase diameter in ACGS for osteoblast behavior

In ACGS specimens, osteoblastic cells in the shallow region of the scaffold exhibited different behavior from that in deep region. In the shallow region, the cells collected the collagen fibrils in the diluted phase (Figure 11A). However, in the deep region, the cells would attach on the interface between concentrated and diluted phases to construct a toroidally aggregating structure, and they collected collagen fibrils to the center of the diluted phase (Figure 11B). Furthermore, the cells attached only on the interface in deeper region of the diluted phase (data not shown). However, osteoblastic cells

uniformly existed in the inner region of ICGS, and such a scaffold structure-dependent cell behavior was not observed in ICGS (Figure 10C, D). The results suggest that morphology of osteoblastic cell would be changed with the diameter of diluted phase. Therefore, if we can control the diameter of the diluted phase, cell behavior in the diluted phase could be controlled. In fact, diameter or number of diluted phase is easily and broadly controlled by changing temperature, ionic strength, pH, and collagen concentration. I confirmed controllability of macroscopic structure of ACGS by changing gelling temperature (Figure 19).

Optical photographs of the thin ACGS films were shown in Figure 19(A)-(C). Irrespective of the gelling temperature, the number of diluted phase ($N_{pore}$) decreased with increasing the distance from the periphery to the center of the thin ACGS film ($r$), whereas the diameter of diluted phase ($D_{pore}$) increased with decreasing $r$. Apparently, $N_{pore}$ decreases with increasing the gelling temperature. The result suggests that $N_{pore}$ can be controlled by the gelling temperature.

Figure 19(D) shows that the $r$ dependences of $D_{pore}$ for the specimens prepared at various temperatures. At the peripheral part of the thin ACGS film (1 mm $\leq r \leq$ 3 mm), there were statistically significant increases in $D_{pore}$ with the increase in r for the specimens prepared at various temperatures. No apparent temperature dependence of $D_{pore}$ was observed. At the center part of the thin ACGS film (5 mm $\leq r \leq$ 7 mm), on the other hand, $D_{pore}$ decreased with increasing the temperature. The results show that the $r$ dependence of $D_{pore}$ is significantly dependent on the gelling temperature. To quantify the positional dependence of $D_{pore}$, I estimated the slope of plots of $D_{pore}$ vs. $r$

($dD_{pore}/dr$). Figure 19(E) shows that the temperature dependence of $dD_{pore}/dr$. $dD_{pore}/dr$ decreased with increasing the temperature. Therefore, I can control the "taper geometry" of diluted and concentrated phases by changing the gelling temperature.

The collagen concentrations in the concentrated and diluted phases could be dependent on the ratio of both phases' volumes. Since the volume of diluted phase increases with increasing $N_{pore}$ and $D_{pore}$, the ratio of both phases' volumes is dependent on $N_{pore}$ and $D_{pore.}$ As shown above, the positional dependences of $N_{pore}$ and $D_{pore}$ can be controlled by the gelling temperature. Therefore, we can control the positional dependence of the ratio of both phases' volumes by changing the gelling temperature. In other words, we can control the positional dependence of the collagen concentration gradient in the concentrated and diluted phases by changing the gelling temperature.

These controllable features of ACGS indicate a high potential ability as a novel scaffold material in tissue engineering.

## 8. Application of scaffold for osteoblast cultivation

To evaluate the functional ability of ACGS for bone-tissue engineering, I investigated the calcification behavior induced by MC3T3-E1 cells on the ACGS. The calcification behavior was evaluated by using the wide angle X-ray diffraction (WAXD) measurement. WAXD profiles for the specimens cultured on the thin ACGS film and the thin ICGS film were shown in Figure 20C and D respectively. Diffraction peaks due to the hydroxyapatite (HAp) crystal were observed in the WAXD profiles for the specimens cultured on the thin ACGS film. The peak intensity increased with the cultivation time. However, no apparent peak was observed in isotropic specimens both day 10 and 21. The

results show that ACGS was a suitable scaffold for bone-tissue engineering, and suggest that the ACGS would promote the calcification by osteoblastic MC3T3-E1 cells.

# Conclusion

Culturing osteoblasts on an anisotropic collagen gel scaffold (ACGS), interaction of cells with the scaffold was investigated focusing on how the scaffold structure was remodeled from molecular rearrangements to macroscopic morphology. As has been expected, cells favored staying in pliant dilute phase in ACGS. The dilute phase is in a tapered cylinder shape along the thickness direction, where the diameter of the dilute phase increased with the depth from the surface. Immediately below the surface of ACGS, where the size of the diluted phase is comparable to that of cells, a cell placed at the center of the phase and looked needleworking with collagen fibers. In the deep region, cells attached on the interface between the diluted and the concentrated phases and aggregated in a toroidal shape. Through the interaction with cells, local packing state of collagen fibers in ACGS was changed. Along with the gradual change in the gel structure, the interaction of cells with the scaffold also changed. I consider the cell function of scaffold contracting force generation after anchoring on the matrix would underlie the phenomena observed.As it is possible to control the structure of ACGS by regulating temparature, ionic strength, pH, and collagen concentration during preparation, the cells-scaffold interaction can be also controllable, which may promise a tailor-made tissue engineering.

# Chapter 2: Multiscale analysis of osteoblastic behavior by application of mechanical stimuli for osteoblasts

## Introduction

The principal functions of bones are to protecting soft organs, and to transmit muscle forces from one part of the body to another. Mechanical properties of bone are those of a strong material that shows high elasticity and high durability. These excellent mechanical properties are derived from complicated and ordered collagen-mineral structure. It has long been recognized that the load application determines the bone morphology, in which the collagen fibers as well as mineral particles are oriented to the principle load direction during a remodeling process by bone cells, in particular osteoblasts.

Osteoblasts are cells known to produce extracellular matrix (ECM) which is composed mainly of Type I collagen. Osteogenesis by osteoblasts has been known to be achieved along with the osteoblast differentiation from its precursor cell. Osteoblasts are also responsible for the mineralization of bone by secreting calcium phosphate such as hydroxyapatite.

Mechanical stimuli (MS) have long been regarded to play an important role for osteoblasts differentiation [13-15]. In previous researches, pre-osteoblastic cells have been cultured in bone-mimic matrices to investigate the effect of MS on osteoblastic differentiation [16-24]. Those cells were exposed to various

kinds of MS modes such as shear, compressive, and tensile forces *in vitro* [14-26].

However, MS effect for osteoblast behavior such as ossification from macroscopic to microscopic scale was not observed in detail.

The aim of this study is to elucidate MS effect for mineral deposition by osteoblasts from macroscopic to microscopic scale. For this purpose, I cultured osteoblastic cells in a collagen sponge, which is developed for MS application for cells. CLSM observation was used to confirm cell attachment and viability and detect macroscopic mineralization by osteoblasts. Furthermore, SAXS and WAXD analysis were performed to detect microscopic change of matrix and calcium deposition.

# Materials & Methods

## 1. Solution preparation

The growth medium was Minimum Essential Medium Alpha (MEM $\alpha$ , Wako) supplemented with 10% FBS (fetal bovine serum; PAA Laboratories, Austria) and 1% penicillin–streptomycin (Sigma Chemicals). The differential medium was the growth medium supplemented with 2 mM glycerophosphate disodium salt pentahydrate (MP Biomedicals) and 50 $\mu$g/ml L-ascorbic acid phosphate magnesium salt n-hydrate (Wako).

For conforcal laser scanning microscope observation, blocking solution, primary antibody solution, secondary antibody solution, Cell viability assay solution and Calcein solution were prepared. The blocking solution consisted of 10% FBS and 0.5% Triton X-100 (Wako) in phosphate buffer saline consisting of 2.3 mM of KCl, 1.5 mM of $KH_2PO_4$, 8.4 mM of $Na_2HPO_4$ and 137 mM of NaCl at pH 7.4 (PBS(-)). An anti-collagen alpha I (SC-8784-R, Santa Cruz) diluted 1:200 in the blocking solution was used as the primary antibody solution. An Alexa Fluor 633-conjugated anti-rabbit IgG (Molecular Probes) diluted 1:1000 in the blocking solution was used as the secondary antibody solution. 300 units of Alexa Fluor 488-conjugated phalloidin (Molecular Probes) solution was diluted 1:60 in PBS(-). Cell viability assay solution is consisted of 1 $\mu$g/ml of Calcein-AM (Dojindo Labolatories, Kumamoto, Japan) and 1 $\mu$g/ml of PI (Dojindo Labolatories) in PBS (-). Calcein solution is consisted of 1 $\mu$g/ml of Calcein (Dojindo Labolatories) in PBS (-).

## 2. Cell culture

The osteoblastic cell line (MC3T3-E1 cells) was provided by RIKEN BRC

through the National Bio-Resource Project of MEXT, Japan. MC3T3-E1 cells were cultured in the growth medium. Cells were cultured on a cell culture plastic dish (FG-2090; Nippon Genetics Co. Ltd, Tokyo, Japan) in an incubator regulated at 37℃ and 5% $CO_2$. Cells at passage 5 were seeded into collagen sponge. In this experiment, I used Atelocollagen sponge MIGHTY® (Koken Co. Ltd.) for cell culture scaffold. The collagen sponge is derived from Bovine dermis Type I atelocollagen, and it has high durability for compressive stress (Max. 30 kPa). Furthermore, its high mechanical strength can eliminate scaffold contraction which is usually observed in osteoblast-seeded collagen gel in long-time cultivation. Therefore, it is suitable for MS application on osteoblasts in 3D condition. This collagen sponge is cylindrical shape, 5 mm in diameter and 3 mm in thickness. Seeding density was $2.0 \times 10^4$ cells/sponge. Two days after seeding, the medium was changed to the differentiation medium. The medium was changed every 3 days. MS applied specimens (MS+) and not applied specimens for control (MS-) were taken from a dish at day 7, day 14, day 21 and day 28, and were used in the following experiments.

## 3. MS application

MS was applied to MC3T3-E1 cells using the MS-application apparatus shown in Figure 4. The device monitors compressive deformation by a deformation sensor in real-time. The device was placed in the 37 ℃ , 5% $CO_2$ incubator. The specimen was set on the stage. A cyclic compressive strain was directly applied to specimens by an aluminum indenter (10 mm in thickness, 30 mm in diameter, cylindrical shape). Strain amplitude and the frequency of MS were controlled at 3 % and 3 Hz, respectively. MS was

applied for 1 h per day from day 0 to day 6.

## 4. Conforcal laser scanning microscope observation

### 4-1 Cell attaching assay

To observe cell adhesion to collagen sponge, collagen molecules and actin fibers in osteoblast were visualized using immunofluorescence staining for collagen molecules and Alexa Fluor 488-conjugated phalloidin for actin fibers, respectively.

Collagen staining: Specimens were washed with PBS(-) three times, then fixed by 4% formaldehyde for 30 min at 4℃. Specimens were blocked and permeated with blocking solution at room temperature for 3 h. Specimens were then incubated with the primary antibody solution overnight at room temperature. Specimens were washed three times with PBS(-), followed by incubation at room temperature for 3 h in the secondary antibody solution.

Actin fiber staining: Specimens were washed three times with PBS(-), and were then treated with phalloidin solution for 3 h.

### 4-2 Cell viability assay

Cell viability was investigated using Calcein-AM and Propidium Iodide (PI) for confirming biocompatibility of collagen sponge at 14 days cultivation. Calcein-AM is a conjugate of Calcein (fluorescent dye) and acetoxymethyl ester residues. Calcein-AM is a non-fluorescent molecule that penetrates the cell membrane, and AM residue is cleaved by cytosolic esterases resulting in intracellular green fluorescence. Therefore, Calcein-AM is used as an index of live cell. PI is an intercalating agent and impermeable molecule. PI is used as an index of dead cells, because cell membrane of the dead cell is broken.

Specimens were washed three times with PBS(-), and were then treated with cell viability assay solution for 1 h. These processes were performed in the 37 ℃, $CO_2$-free incubator.

### 4-3 Calcium staining

To detect MS effect on calcium deposition by osteoblast in the collagen sponge, calcium ions were stained by Calcein solution.

Specimens cultured with 21 days and 28 days were washed three times with PBS(-), and then treated with Calcein solution for 1 h. These processes were performed in the 37 ℃, $CO_2$-free incubator.

All specimens were mounted on a coverslip and observed by a confocal laser scanning microscope (CLSM; Leica TCS SP5).

## 5. SAXS and WAXD measurements

SAXS and WAXD measurements were concurrently performed at the BL40B2 beam line equipped in the SPring-8 (Japan Synchrotron Radiation Research Institute; JASRI). The X-ray wavelength was 1.5 Å. The scheme of optical system is shown in Figure 21. SAXS patterns were acquired with a CCD (C4880, Hamamatsu Photonics, Japan) equipped with an X-ray imaging intensifier (IV4554P, Hamamatsu Photonics), and sample-to-detector distance was 4250 mm. WAXD patterns were obtained by flat panel detector (C9728DK, Hamamatsu Photonics), and sample-to-detector distance was 62.91mm. We selected the proper exposure time for each specimen to prevent a saturating scattering intensity. Exposure times were 100 ms in SAXS experiment and 5 s in WAXD experiment, respectively. All experiments were performed at 37 ℃. 2D SAXS and WAXD patterns were corrected by

subtracting the dark current of the detector. To obtain 1D SAXS profiles, the circular average of 2D SAXS patterns were calculated. The averaged scattering intensity I(q) was plotted as a function of scattering vector q, defined as $q = (4\pi / \lambda)\sin(2\theta/2)$, where $2\theta$ is the scattering angle. 1D WAXD profiles were obtained by FIT2D (Andy Hammersley).

# Results and Discussion

## 1. Cell attachment assay

To observe cell adhesion to collagen sponge, collagen molecules and actin fibers in osteoblastic cells were visualized using immunofluorescence staining (Figure 21). Actin fibers in osteoblastic cell were observed on the surface of the collagen sponges in both MS- (Figure 22A) and MS+ (Figure 22B) specimens. These results confirm that the collagen sponge has good cell attachment ability and it is suitable for osteoblastic cell culture.

Cell distribution was not changed between MS- and MS+ specimens, which suggest that MS application is not harmful for osteoblastic cell and not affecting cell distribution or cell proliferation.

## 2. Cell viability assay

Biocompatibility of the collagen sponge was further confirmed by cell viability assay (Figure 23). Almost all cells lived in both MS- and MS+ specimens. This result suggests that the collagen sponge has a high biocompatibility and cells were not damaged by MS application.

## 3. Calcium staining

To investigate MS effect for calcium deposition by osteoblastic cell, calcium ions were stained by Calcein (Figure 24, 25). Calcein is a calcium-binding fluorescent dye, and it is an impermeable molecule. In MS+ specimen, spheroidal calcium particles (arrow head) were observed at 21 days cultivation (Figure 24A). However, this spheroidal calcium particles were not detected in MS- specimen (Figure 24B). Spheroidal calcium particles were observed in both specimens at 28 days cultivation (Figure 24), but

fluorescent intensity of MS+ specimen was much higher than that of MS-. In MS- specimens, weak calcium deposition was observed, but the staining pattern was almost same. This spheroidal calcium particle might be a calcospherite. These results suggest that MS only accelerate calcospherite deposition by osteoblastic cell. If MS- specimens were cultured longer time, stronger calcium deposition same as MS+ specimens would be observed.

## 4. SAXS measurements

2D SAXS patterns for Scaffold (dried and acellular collagen sponge or MS- and MS+ cultured 7, 14, 21 and 28 days are shown in Figure 26. An isotropic scattering pattern was observed in all specimens. This isotropic pattern would be derived from isotropic structure of the collagen sponge in sub-micrometer level.

Log-log plots of SAXS profiles for Scaffold, MS+ and MS- specimens are shown in Figure 27 and 28, respectively. The logarithm of I(q) for all specimens linearly decreased with an increasing logarithm of q, and change of the slope was not observed in each specimens. Changes in slope value (*a*) of Scaffold or MS+ and MS- specimens along with the cultivation time are shown in Figure 29. The slope value of the Scaffold is 3.4. Other cell-seeded specimens are about 4, and change of the slope is not observed in with or without MS and time course of culture. This result suggests that not MS application but osteoblastic cell seeding might affect the structure of the scaffold. However, condition of the specimens was different. Scaffold is completely dried, but other specimens were slightly wet. This difference of the water content in the specimens might affect the result.

Since the values of *a* were in the range of 3 to 4, the values of *a* are related

to the surface fractal dimension, $D_s$. In this case, the value of $D_s$ was almost 2.5 (Scaffold) and 2 (other specimens). This result indicates that the surface of the scattering bodies in cell-seeded specimens would be very smooth, and osteoblastic cell might be changed and flattened the surface of the scaffold. However, MS effect was not observed in all specimens. Collagen fiber density is extremely high in the collagen sponge; scattering behavior is dominated by matrix collagen. Therefore, effect of cell matrix remodeling might be too weak to detect.

## 5. WAXD measurements

2D WAXD patterns for Scaffold or MS+ and MS- cultured 7, 14, 21 and 28 days are shown in Figure 30.

1D WAXD profiles of MS+ and MS- specimen are shown in Figure 31 and 32. Almost same profiles were observed for all cell-seeded specimens, weak peak was observed at $2\theta = 31^\circ$. This peak (D-spacing is 0.29 nm) is relates to the helical rise per residue in collagen molecule, which is the distance between the amino acid residues along the collagen triple helices. Therefore, cell-seeded specimens would contain collagen molecule. In contrast, no apparent peak was observed in Scaffold. This means that collagen triple helical conformation would be degraded in the scaffold.

MS effect on collagen peak was not observed. Osteoblasts secret collagen at early differentiation stage, therefore MS might not enhance collagen secretion.

Along with the osteoblast calcium deposition, calcium phosphate such as hydroxyapatite had been expected to emerge in the WAXD profile. However,

no peak was observed which attribute to mineral particles. Osteoblastic cells would secret calcium ions as observed in calcium staining. These results suggest that crystalinity of cell-secreted mineral particles might be not good or amount of the mineral particle might be not enough to detect by WAXD analysis. To remove minerals contained in medium, specimens were washed several times with MilliQ water. This treatment may affect the results because cell-secreted mineral particles might be dissolved by washing.

# Conclusion

MS application effect was investigated through macro- and microscopic morphology observations, focusing on collagen remodeling and calcium deposition. For this purpose, osteoblastic cells were cultured in a collagen sponge. MS application was accelerated osteoblastic cell calcium secretion in macroscopic view. However, microscopic structure changing or calcium deposition was not altered by MS application. Optimization of MS application might be needed to adequate enhancement of osteoblast functions.

# References

(1) Langer, R.; Vacanti, J. P. Tissue engineering. *Science* **1993**, 260 (5110), 920–926.

(2) Kunz-Schughart, L. A.; Wenninger, S.; Neumeier, T.; Seidl, P.; Knuechel, R. Three-dimensional tissue structure affects sensitivity of fibroblasts to TGF-beta 1. *Am. J. Physiol. Cell Physiol.* **2003**, 284 (1), 209–219.

(3) Kleinman, H. K.; Philp, D.; Hoffman, M. P. Role of the extracellular matrix in morphogenesis. *Curr. Opin. Biotechnol.* **2003**, 14 (5), 526–532.

(4) Chen, S. S.; Falcovitz, Y. H.; Schneiderman, R.; Maroudas, A; Sah, R. L. Depth-dependent compressive properties of normal aged human femoral head articular cartilage: relationship to fixed charge density. *Osteoarthr. Cartil.* **2001**, 9 (6), 561–569.

(5) Jung, T.-K.; Matsumoto, H.; Abumiya, T.; Masahashi, N.; Kim, M.-S.; Hanada, S.; Mechanical properties-graded Ti Alloy implants for orthopedic applications. *Mat. Sci. Forum* **2010,** 631-632, 205-210

(6) Lanfer, B.; Seib, F. P.; Freudenberg, U.; Stamov, D.; Bley, T.; Bornhäuser, M.; Werner, C. The growth and differentiation of mesenchymal stem and progenitor cells cultured on aligned collagen matrices. *Biomaterials* **2009**, 30 (30), 5950–5958.

(7) Lai, E. S.; Anderson, C. M.; Fuller, G. G. Designing a tubular matrix of oriented collagen fibrils for tissue engineering. *Acta biomaterialia* **2011**, 7 (6), 2448–56.

(8) Isobe, Y.; Kosaka, T.; Kuwahara, G.; Mikami, H.; Saku, T.; Kodama, S. Ori-

ented Collagen Scaffolds for Tissue Engineering. **Materials** *2012*, 5 (3), 501–511.

(9) Mikami, H.; Kuwahara, G.; Nakamura, N.; Yamato, M.; Tanaka, M.; Kodama, S. Two-layer tissue engineered urethra using oral epithelial and muscle derived cells. *J. Urol.* **2012**, 187 (5), 1882–9.

(10) Caliari, S. R.; Weisgerber, D. W.; Ramirez, M. A; Kelkhoff, D. O.; Harley, B. A. C. The influence of collagen-glycosaminoglycan scaffold relative density and microstructural anisotropy on tenocyte bioactivity and transcriptomic stability. *J. Mech. Behav. Biomed. Mater*. **2012**, 11, 27–40.

(11) Guido, S.; Tranquillo, R. T. A methodology for the systematic and quantitative study of cell contact guidance in oriented collagen gels. Correlation of fibroblast orientation and gel birefringence. *J. Cell Sci.* **1993**, 105 (Pt2), 317–331.

(12) Furusawa, K.; Sato, S.; Masumoto, J.; Hanazaki, Y.; Maki, Y.; Dobashi, T.; Yamamoto, T.; Fukui, A.; Sasaki, N. Studies on the formation mechanism and the structure of the anisotropic collagen gel prepared by dialysis-induced anisotropic gelation. *Biomacromolecules* **2012**, 13 (1), 29–39; corrections, *Biomacromolecules* **2012**, 13 (4), 1232–1232.

(13) Sudo, H.; Kodama, H.; Amagai, Y.; Yamamoto, S.; Kasai, S. In vitro differentiation and calcification in a new clonal osteogenic cell line derived from newborn mouse calvaria. *J. Cell Biol.* **1983**, 96 (1), 191–198.

(14) Robling, A. G.; Castillo, A. B.; Turner, C. H. Biomechanical and molecular regulation of bone remodeling. *Annu. Rev. Biomed. Eng.* **2006**, 8, 455–498.

(15) Duncan, R. L.; Turner, C. H. Mechanotransduction and the functional

response of bone to mechanical strain. *Calcif. Tissue Int.* **1995**, 57 (5), 344–358.

(16) Rubin, J.; Rubin, C.; Jacobs, C. R. Molecular pathways mediating mechanical signaling in bone. *Gene* **2006**, 367 (15), 1–16.

(17) Kapur, S.; Baylink, D. J.; Lau, K. H. Fluid flow shear stress stimulates human osteoblast proliferation and differentiation through multiple interacting and competing signal transduction pathways. *Bone* **2003**, 32 (3), 241–251.

(18) Datta, N.; Pham, Q. P.; Sharma, U.; Sikavitsas, V. I.; Jansen, J. A.; Mikos, A. G. In vitro generated extracellular matrix and fluid shear stress synergistically enhance 3D osteoblastic differentiation. *Proc. Natl. Acad. Sci. U.S.A.* **2006**, 103 (8), 2488–2493.

(19) Bancroft, G. N.; Sikavitsas, V. I.; van den Dolder, J.; Sheffield, T. L.; Ambrose, C. G.; Jansen, J.A.; Mikos, A. G. Fluid flow increases mineralized matrix deposition in 3D perfusion culture of marrow stromal osteoblasts in a dose-dependent manner. *Proc. Natl. Acad. Sci. U.S.A.* **2002**, 99 (20), 12600–12605.

(20) Walker, L. M.; Publicover, S. J.; Preston, M. R.; Said Ahmed, M. A.; El Haj, A. J. Calciumchannel activation and matrix protein upregulation in bone cells in response to mechanical strain. *J. Cell. Biochem.* **2000**, 79 (4), 648–661.

(21) Liu, J.; Liu, T.; Zheng, Y.; Zhao, Z.; Liu, Y.; Cheng, H.; Luo, S.; Chen, Y. Biochem. Early responses of osteoblast-like cells to different mechanical signals through various signaling pathways. *Biochem. Biophys. Res. Commun.* **2006**, 348 (3), 1167–1173.

(22) Rath, B.; Nam, J.; Knobloch, T. J.; Lannutti, J. J.; Agarwal, S. Compressive forces induce osteogenic gene expression in calvarial osteoblasts. *J. Biomech.*

**2008**, 41 (5), 1095–1103.

(23) Ziros, P. G.; Gil, A. P.; Georgakopoulos, T.; Habeos, I.; Kletsas, D.; Basdra, E. K.; Papavassiliou, A.G. Papavassiliou AG. The bone-specific transcriptional regulator Cbfa1 is a target of mechanical signals in osteoblastic cells. J. *Biol. Chem.* **2002**, 277 (26), 23934–23941.

(24) Tang, S. Y.; Herber, R.-P.; Ho, S. P.; Alliston, T. Matrix metalloproteinase-13 is required for osteocytic perilacunar remodeling and maintains bone fracture resistance. *J. Bone Miner. Res.* **2012**, 27 (9), 1936–1950.

(25) Guo, Y.; Zhang, C.; Zeng, Q.; Li, R.; Liu, L.; Hao, Q.; Shi, C.; Zhang, X.; Yan, Y. Mechanical strain promotes osteoblast ECM formation and improves its osteoinductive potential. *Biomed. Eng. Online* **2012,** 11, 80.

(26) Li, Y.; Ge, C.; Long, J. P.; Begun, D. L.; Rodriguez, J. A; Goldstein, S. A; Franceschi, R. T. Biomechanical stimulation of osteoblast gene expression requires phosphorylation of the RUNX2 transcription factor. *J. Bone Miner. Res*. 2012, 27 (6), 1263–1274.

(27) Maki, Y.; Ito, K.; Hosoya, N.; Yoneyama, C.; Furusawa, K.; Yamamoto, T.; Dobashi, T.; Sugimoto, Y.; Wakabayashi, K. Anisotropic structure of calcium-induced alginate gels by optical and small-angle X-ray scattering measurements. *Biomacromolecules* **2011**, 12 (6), 2145–2152.

(28) Engler, A. J.; Sen, S.; Sweeney, H. L.; Discher, D. E. Matrix elasticity directs stem cell lineage specification. *Cell* **2006**, 126 (4), 677–689.

(29) Guilak, F.; Cohen, D. M.; Estes, B. T.; Gimble, J. M.; Liedtke, W.; Chen, C. S. Control of stem cell fate by physical interactions with the extracellular matrix. *Cell Stem Cell* **2009**, 5 (1), 17–26.

(30) Reilly, G. C.; Engler, A. Intrinsic extracellular matrix properties regulate stem cell differentiation. J. *J. Biomech.* **2010**, 43 (1), 55–62.

(31) Davis, G. E.; Senger, D. R. Endothelial extracellular matrix: biosynthesis, remodeling, and functions during vascular morphogenesis and neovessel stabilization. *Circ. Res.* **2005**, 97 (11), 1093–1107.

(32) Shieh, A. C.; Rozansky, H.A; Hinz, B.; Swartz, M. A. Tumor cell invasion is promoted by interstitial flow-induced matrix priming by stromal fibroblasts. *Cancer Res.* **2011**, 71 (3), 790–800.

(33) Menon, S.; Beningo, K. A. Cancer cell invasion is enhanced by applied mechanical stimulation. *PLoS One* **2011**, 6 (2), e17277.

(34) Martin J. E.; Hurd, A. J. Scattering from fractals. *J. Appl. Cryst.* 1987, 20, 61–78

(35) Glatter, O.; Kratky, O. *Small Angle X-ray Scattering,* Academic Press, London, 1982

(36) Wood, G. C.; Keech, M. K. The formation of fibrils from collagen solutions 1. The effect of experimental conditions: kinetic and electron-microscope studies. *Biochem. J.* **1960**, 75 (3), 588-598;

(37) Raub, C. B.; Suresh, V.; Krasieva, T.; Lyubovitsky, J.; Mih, J. D.; Putnam, A. J.; Tromberg, B. J.; George, S. C. Noninvasive assessment of collagen gel microstructure and mechanics using multiphoton microscopy. *Biophys. J.* **2007**, 92 (6), 2212–2222

(38) Garstenfeld, L. C., Riva, A.; Hodgens, K.; Eyre, D. R.; Landis W.J. Post-translational control of collagen fibrillogenesis in mineralizing cultures of

chick osteoblasts *J. Bone Miner. Res.* **1993**, 8 (9), 1031–1043

(39) Patel, M. J.; Chang, K. H.; Sykes, M. C.; Talish, R.; Rubin, C.; Jo, H. Low magnitude and high frequency mechanical loading prevents decreased bone formation responses of 2T3 preosteoblasts. *J. Cell. Biochem.* **2009**, 106 (2), 306–316.

(40) Dumas, V.; Ducharne, B.; Perrier, A.; Fournier, C.; Guignandon, A.; Thomas, M.; Peyroche, S.; Guyomar, D.; Vico, L.; Rattner, A. Extracellular matrix produced by osteoblasts cultured under low-magnitude, high-frequency stimulation is favorable to osteogenic differentiation of mesenchymal stem cells. *Calcif Tissue Int*. **2010**, 87 (4), 351–364.

(41) Dumas, V.; Perrier, A.; Malaval, L.; Laroche, N.; Guignandon, A.; Vico, L.; Rattner, A. The effect of dual frequency cyclic compression on matrix deposition by osteoblast-like cells grown in 3D scaffolds and on modulation of VEGF variant expression. *Biomaterials* **2009**, 30 (19), 3279–3288.

(42) Kreke, M. R.; Sharp, L. A.; Lee, Y. W.; Goldstein, A. S. Effect of Intermittent shear stress on mechanotransductive signaling and osteoblastic differentiation of bone marrow stromal cells. *Tissue Eng. Part A* **2008**, (14), 529-537.

# Acknowledgements

First of all, I would like to thank for gratefully acknowledgement the supervision of Prof. Naoki Sasaki. I appreciate his gentle guidance and encouragement for my study. I also would like to thank for support of Assoc. Prof. Akimasa Fukui, especially in biological experiment guidance. I appreciate Assist. Prof. Kazuya Furusawa for his frequent communication and supervising of my research. I thank to Prof. Gong for evaluation of my thesis.

I thank Mr. Yoshihiro Ookubo to his speedy and precise response to my laboratory reagent order.

I thank all members of Laboratory of Polymer and Tissue Science for daily communication. I spent a confortable and enjoyable time in my laboratory.

Finally, I am truly thankful for my family. I could not get a Ph.D without financial support of my school fees.

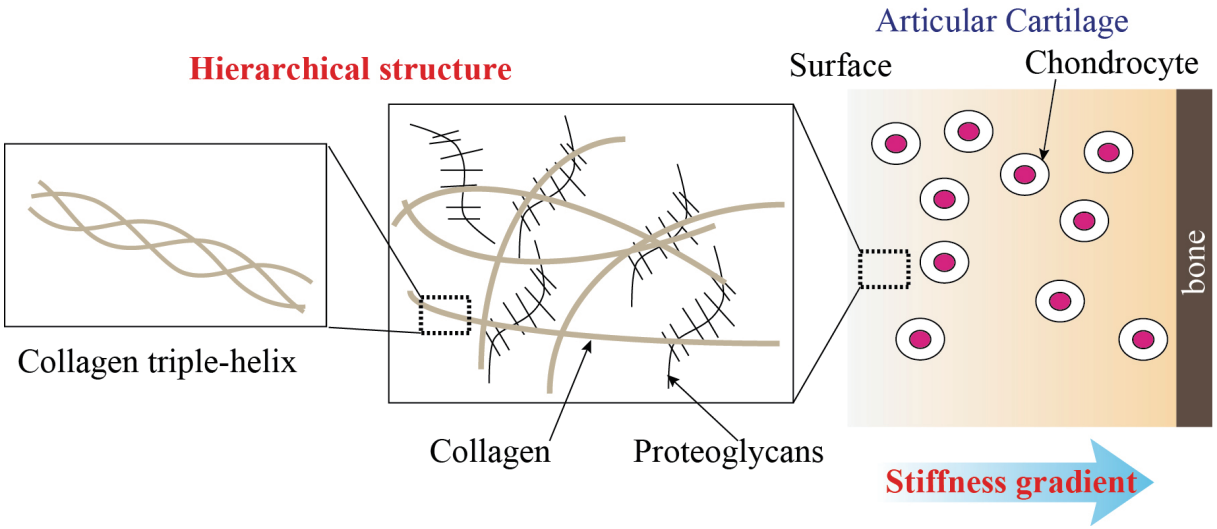


**Figure 1.** Hierarchical structure and property gradient in native cartilage tissue. In macroscopic view (right), chondrocytes exist separately existed in cartilage matrix. More magnified view (middle), collagen fibers and proteoglycans are observed. Collagen fibers are composed of a collagen molecule (left). Collagen molecule is consisted of triple-helix structure of collagen chain. This hierarchical structure (Tissue - cell - fiber - morecule - chain) is important for cartilage function and mechanical properties.

Cartilage has also a property gradient (right). Chen *et al*. found that cartilage elastic modulus was changed from surface to deep region[4]. This change of elastic modulus made stiffness gradient, it also affect cartilage function and chondrocyte through cell-ECM interaction.

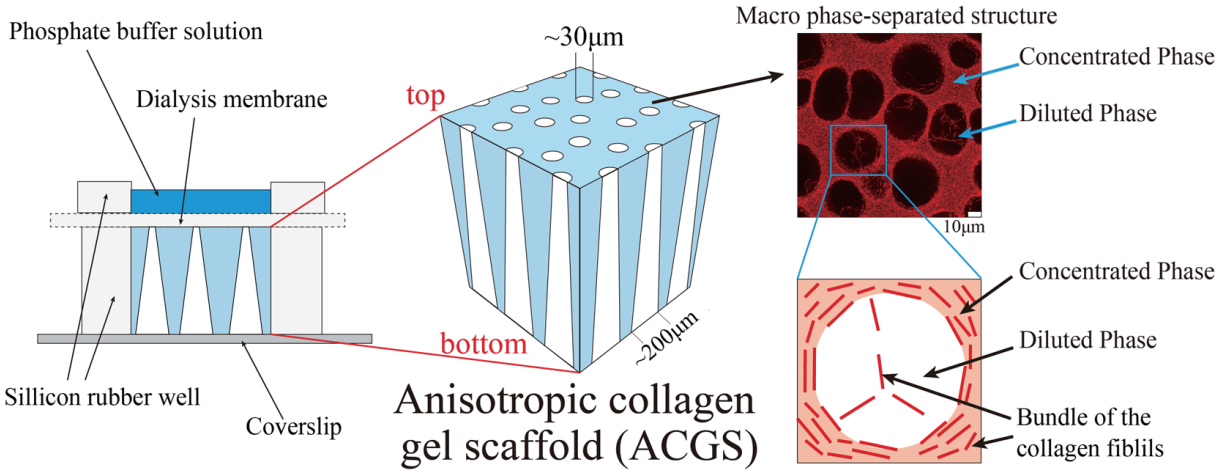


**Figure 2.** Schematic diagram of anisotropic collagen gel scaffold (ACGS). ACGS is prepared from collagen solution and phosphate buffer solution (PBS). The gel has a macro phase-separated structure. It has a high collagen concentration region (concentrated phase) and a low collagen concentration region (diluted phase). Diameter of the diluted phase is gradually changed about 30-200 μm from top to bottom of the gel. Magnified schematic of ACGS shows that collagen fibrils were oriented circumferentially to the interface and diluted phase is not empty space but small number of the bundle of the collagen fibrils is existed. Scale bar = 10 μm

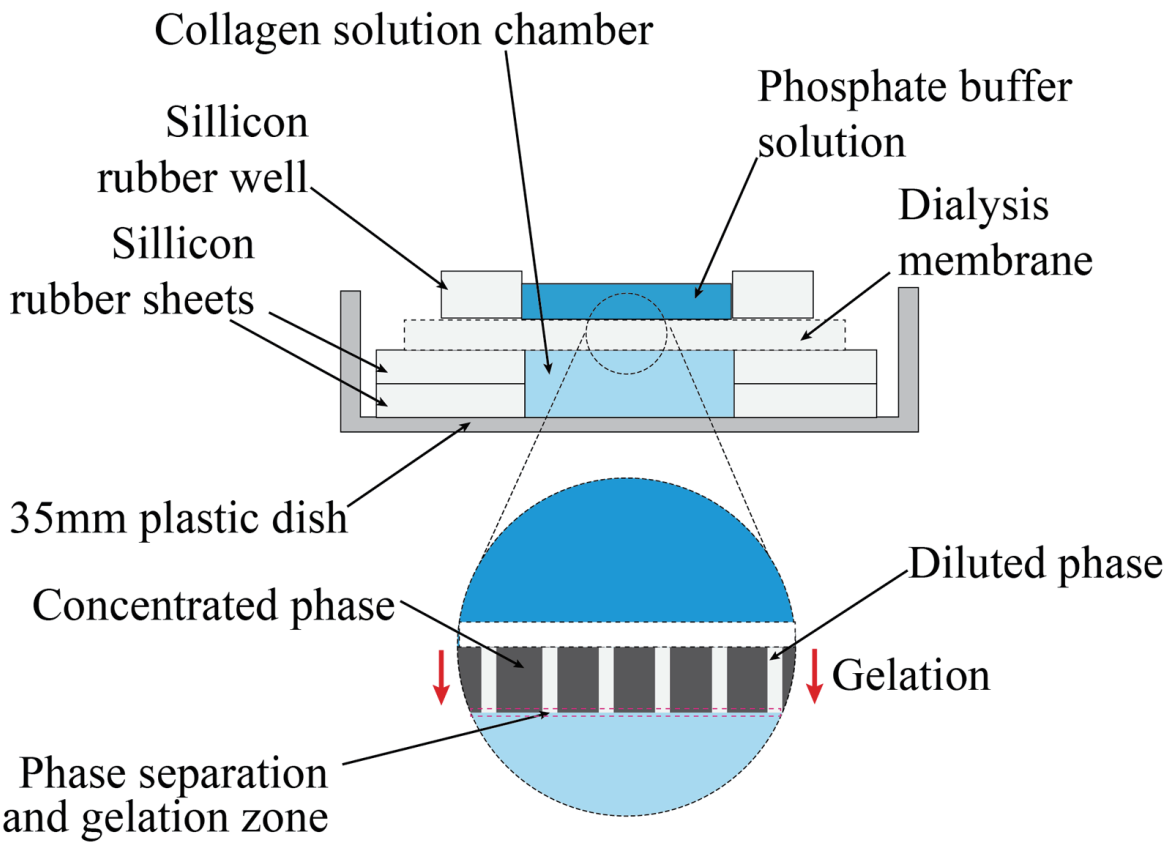


**Figure 3.** Scheme of anisotropic and isotropic gel formation.

The dialysis chamber consisted of two 1.5 mm thickness silicon rubber sheets and put on a 35 mm plastic dish. Both silicon rubbers have a 10 mm circular hole. A total of 200 µl collagen solution was injected into the dialysis chamber. A dialysis membrane was set on the top of the collagen solution chamber, and then the silicon rubber well was put on the dialysis membrane. PBS was poured over the silicon rubber well to make ACGS. Growth medium was poured over the silicon rubber well to make ICGS. During the dialysis process of the collagen solution against PBS or the growth medium, the collagen gel phase grew from the dialysis membrane from the top to the bottom of the dialysis chamber.

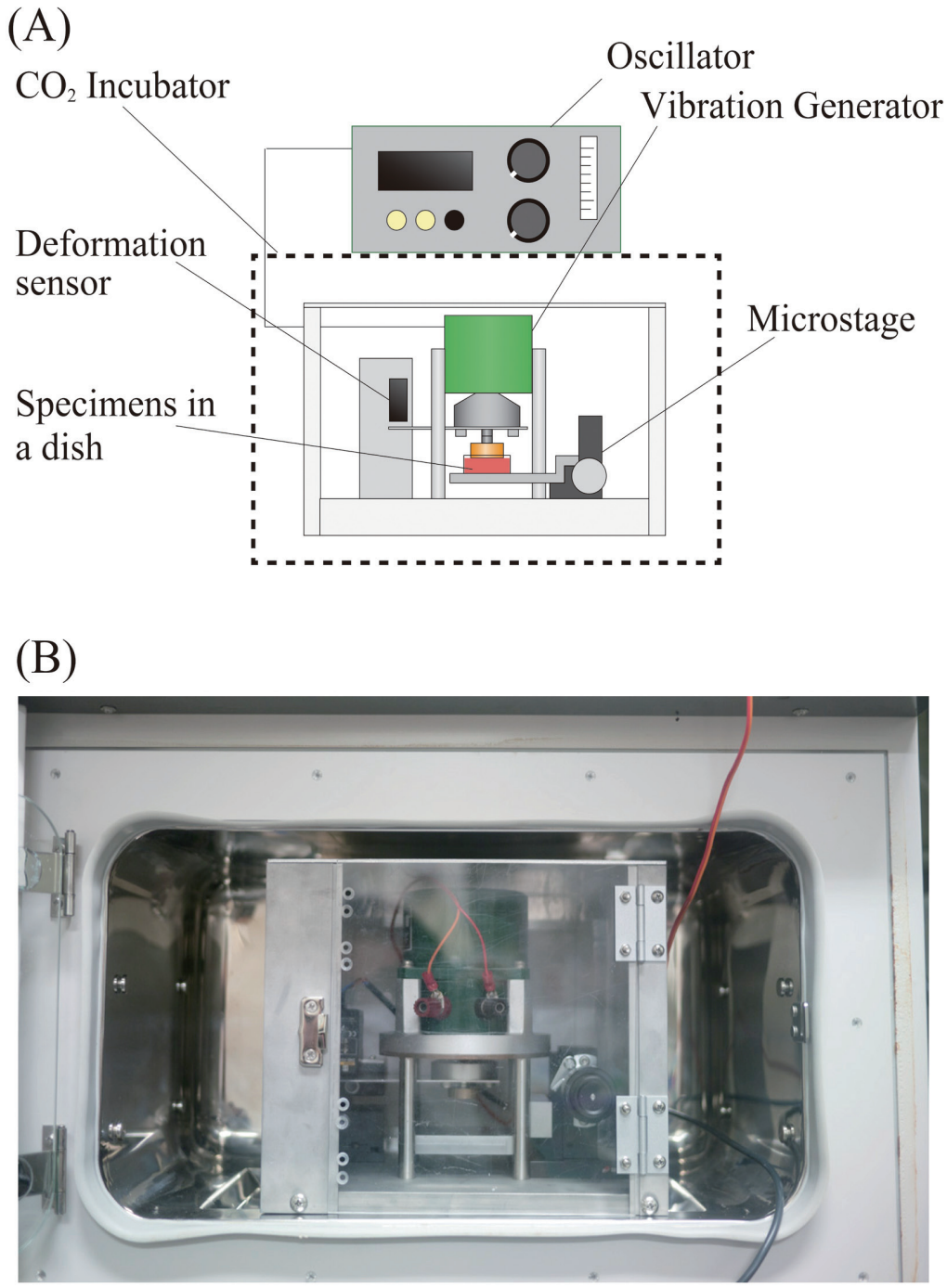


**Figure 4.** Scheme (A) and a picture (B) of the MS application apparatus.

The device was placed in the 37℃, 5% $CO_2$ incubator. The deformation sensor monitors the deformation of a specimen in real-time. The oscillator and vibration generator make a sigmoidal movement of the aluminum indenter. The aluminum indenter is 10 mm in thickness, 30 mm in diameter, with disk shape. The specimen was set on the stage. A periodic compressive strain was directly applied to specimens by the aluminum indenter.

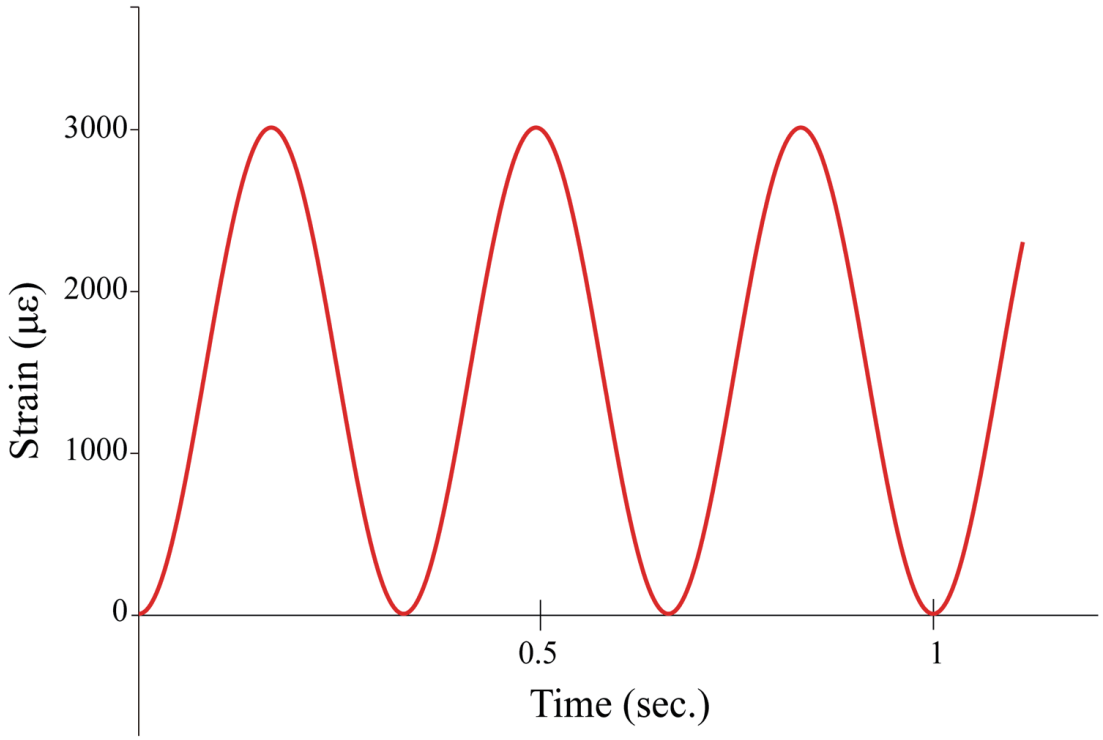


**Figure 5.** Scheme of applied strain amplitude to cell-gel composites.

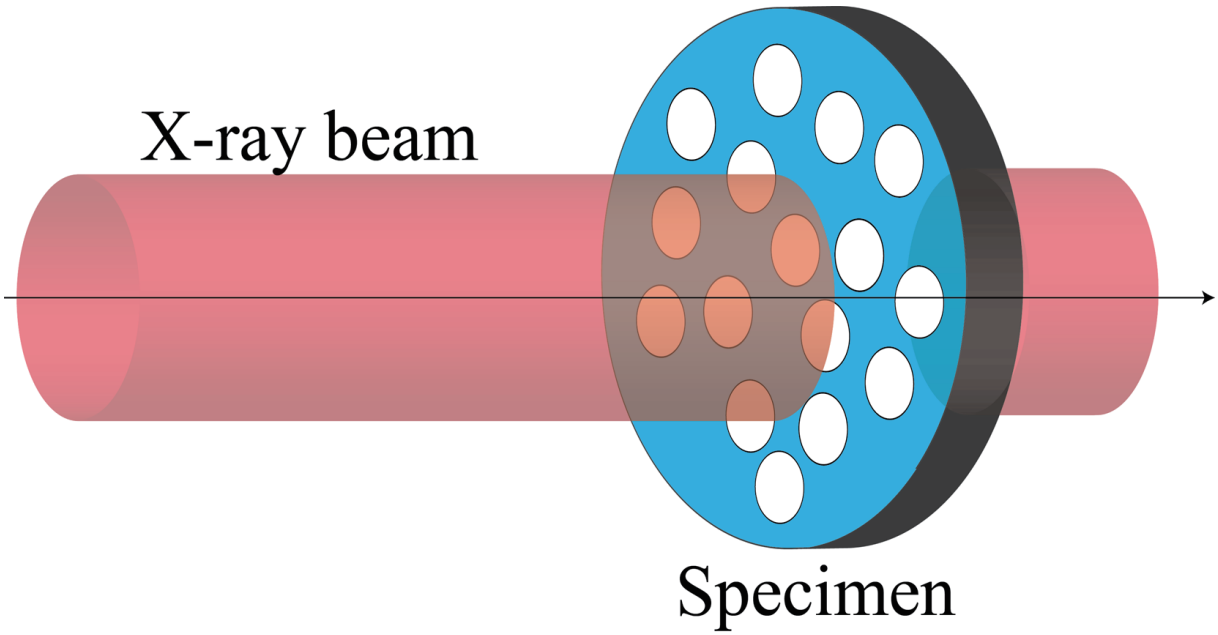


**Figure 6.** Scheme of X-ray beam irradiation to a specimen.

White circles in the specimen disk are dilute phases, which are extending along the thickness direction of the disk.

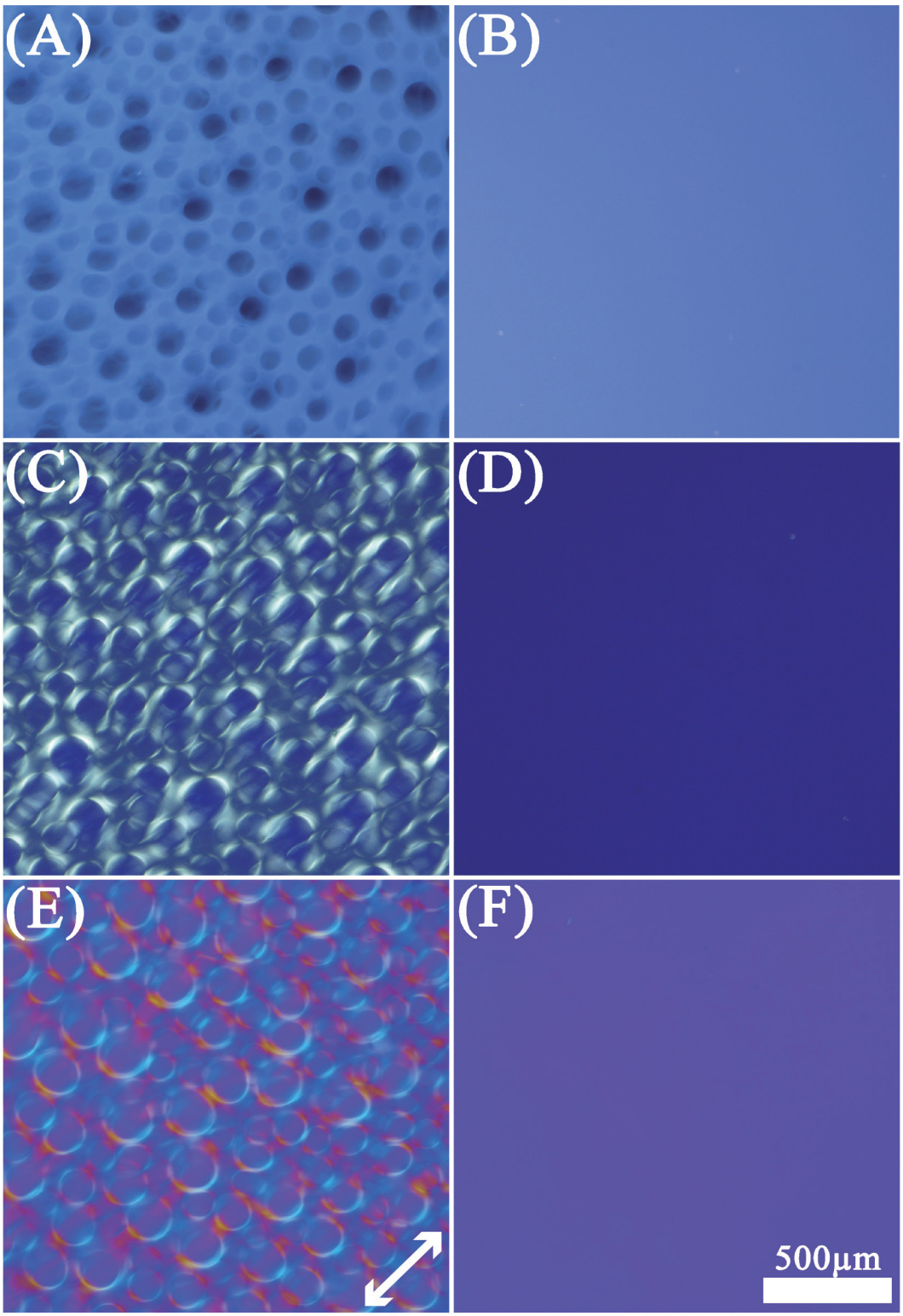


**Figure 7.** Macroscopic morphology of ACGS and ICGS

Specimens observed under a natural light (A, B), polarized light (C, D), and circular polarized light (E, F), respectively. A, C, and E are images of ACGS, and B, D, and F are images of ICGS. Arrow represents the slow axis of quarter-wave plate. Scale bar = 500 μm

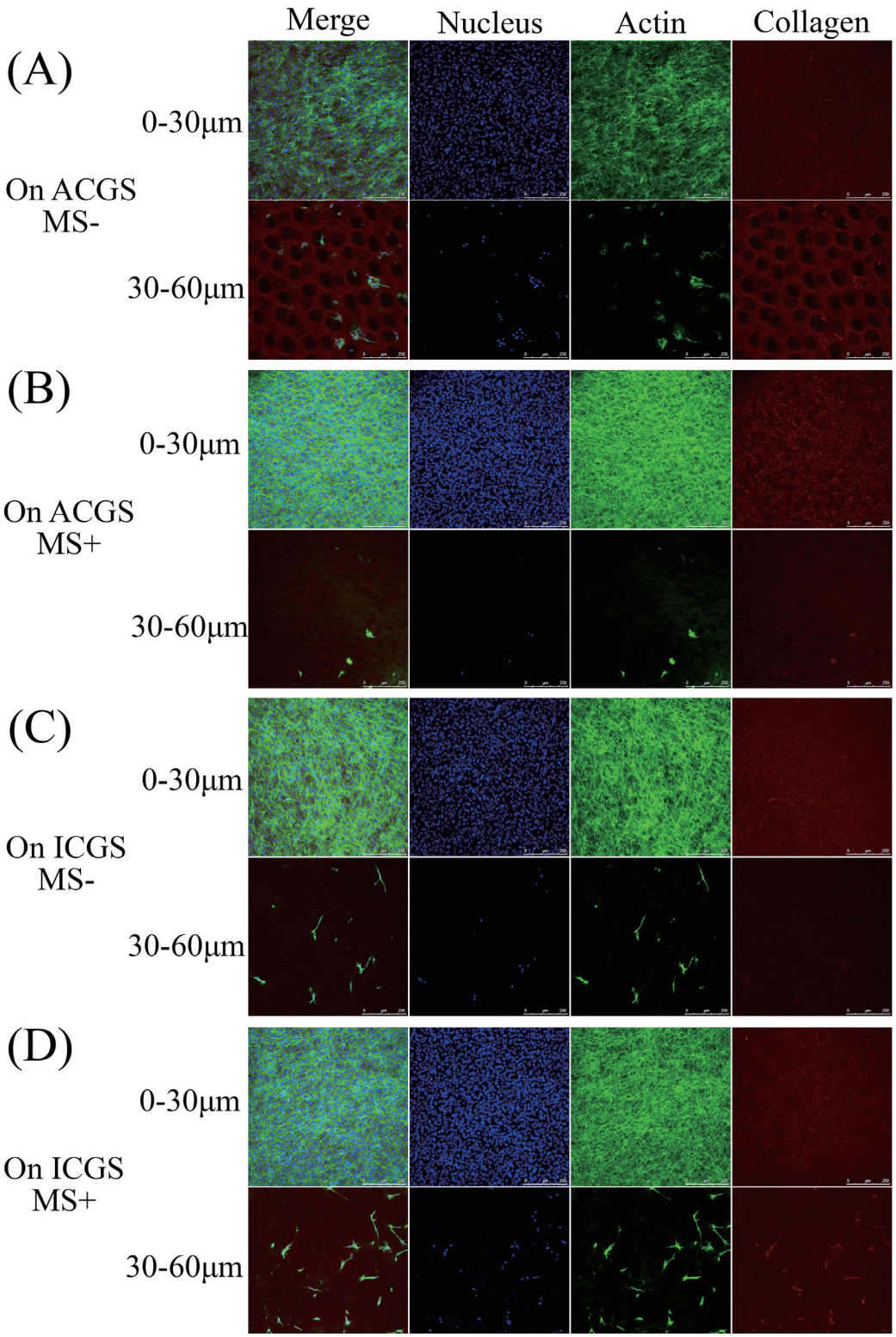


**Figure 8.** CLSM images of the cell-gel composites at 7 days cultivation. (A-D) Low-magnified CLSM images of surface or inner region of each specimen. (A) ACGS-MS, (B) ACGS-MS+, (C)ICGS-MS-, and (D) ICGS-MS+ each at 7 days cultivation. The surface region is 0-30 μm, and 30-60 μm is the inner region of each specimen. Scale bar = 250 μm.

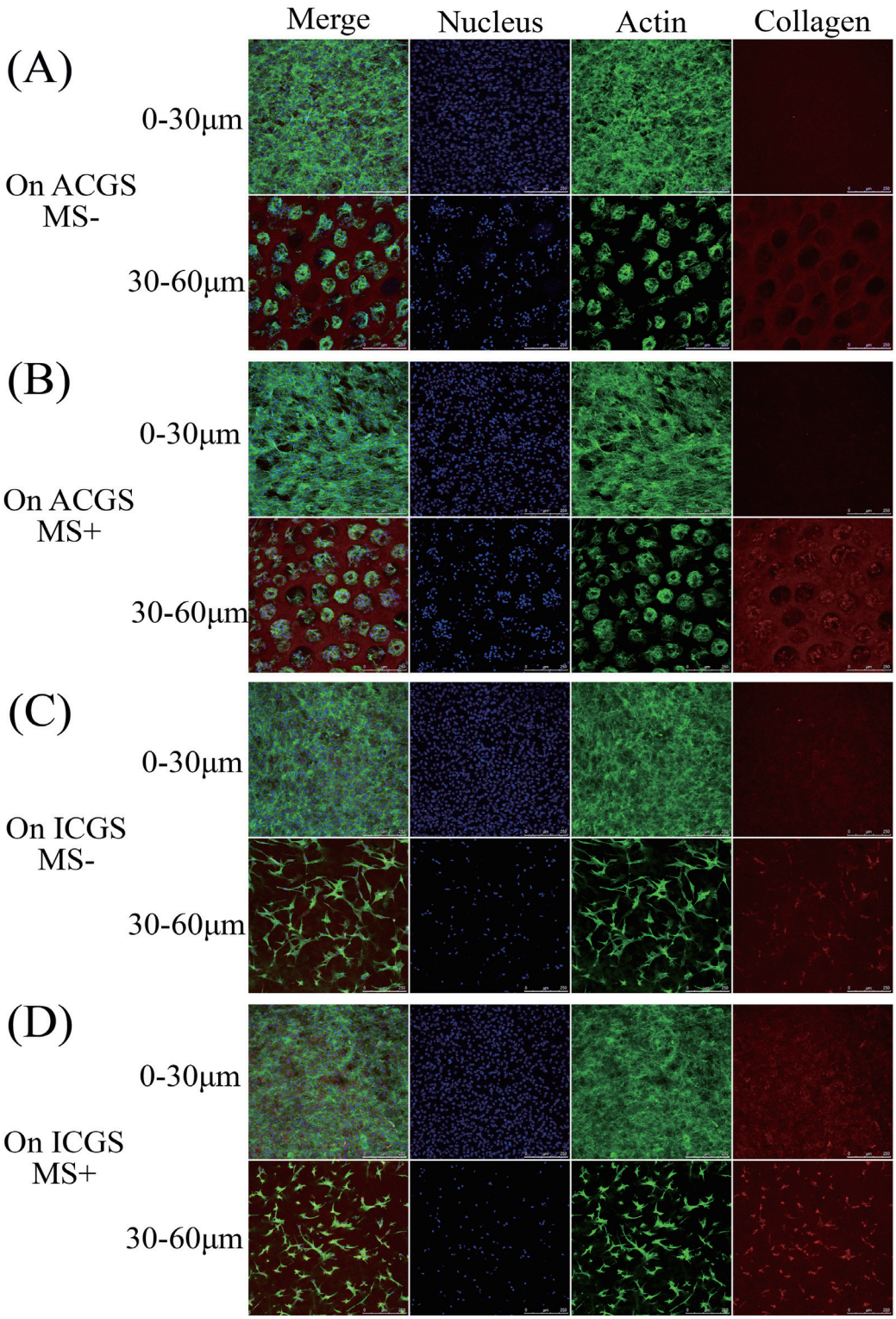


**Figure 9.** CLSM images of the cell-gel composites at 14 days cultivation. (A-D) Low-magnified CLSM images of surface or inner region of each specimen. (A) ACGS-MS, (B) ACGS-MS+, (C)ICGS-MS-, and (D) ICGS-MS+ each at 14 days cultivation. The surface region is 0-30 μm, and 30-60 μm is the inner region of each specimen. Scale bar = 250 μm.

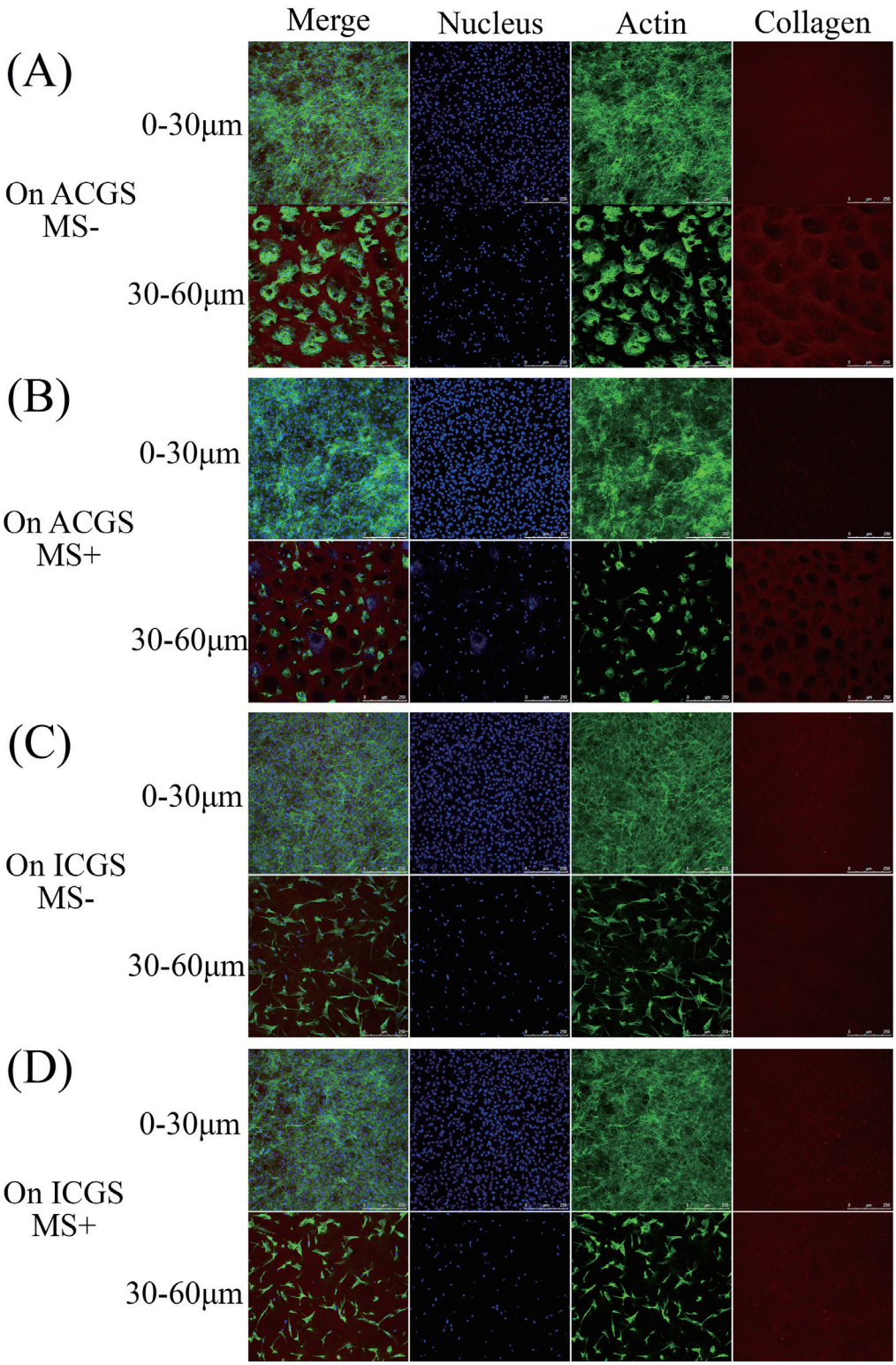


**Figure 10.** CLSM images of the cell-gel composites at 21 days cultivation. (A-D) Low-magnified CLSM images of surface or inner region of each specimen. (A) ACGS-MS, (B) ACGS-MS+, (C)ICGS-MS-, and (D) ICGS-MS+ each at 21 days cultivation. The surface region is 0-30 μm, and 30-60 μm is the inner region of each specimen. Scale bar = 250 μm.

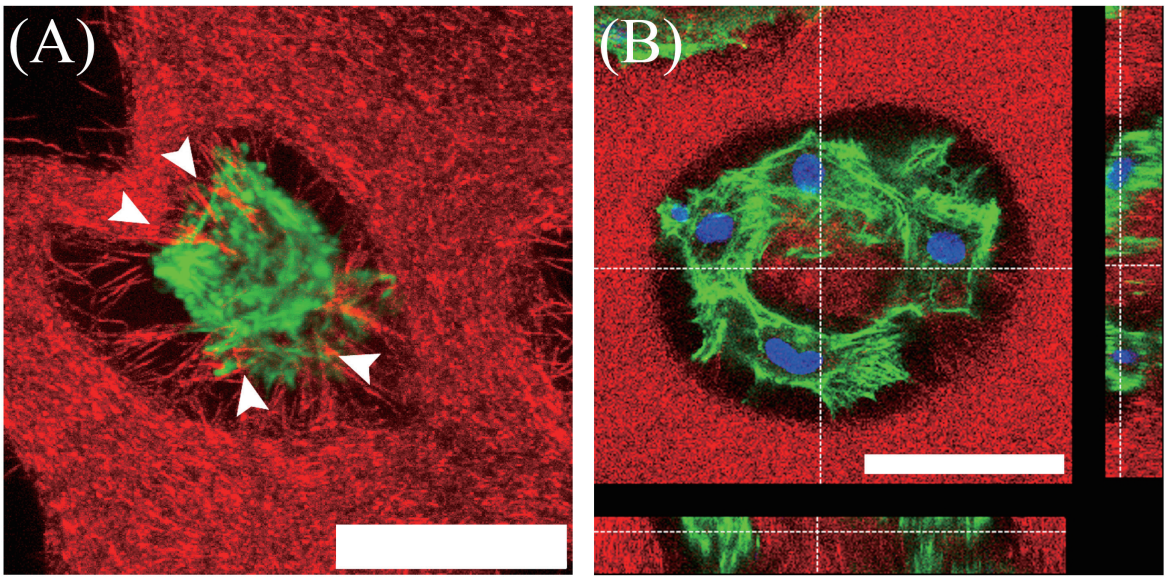


**Figure 11.** Magnified CLSM images of the cell-gel composites.

(A) Z-stack magnified image of osteoblasts in the diluted phase of ACGS-MS- at 7 days cultivation. Red: Collagen, Green: Actin fibers. Osteoblasts looked pulling collagen fibers from the interfacial wall between concentrated and diluted phases in the diluted phase of ACGS (arrow heads). Scale bar = 25 μm (B) Z-stack magnified image of osteoblasts in the diluted phase of ACGS-MS- at 14 days cultivation. Red: Collagen, Blue: Nuclei, and Green: Actin fibers. Osteoblasts made tolloidary structure, and they collected collagen fibers in the center of the diluted phase. Scale bar = 25μm.

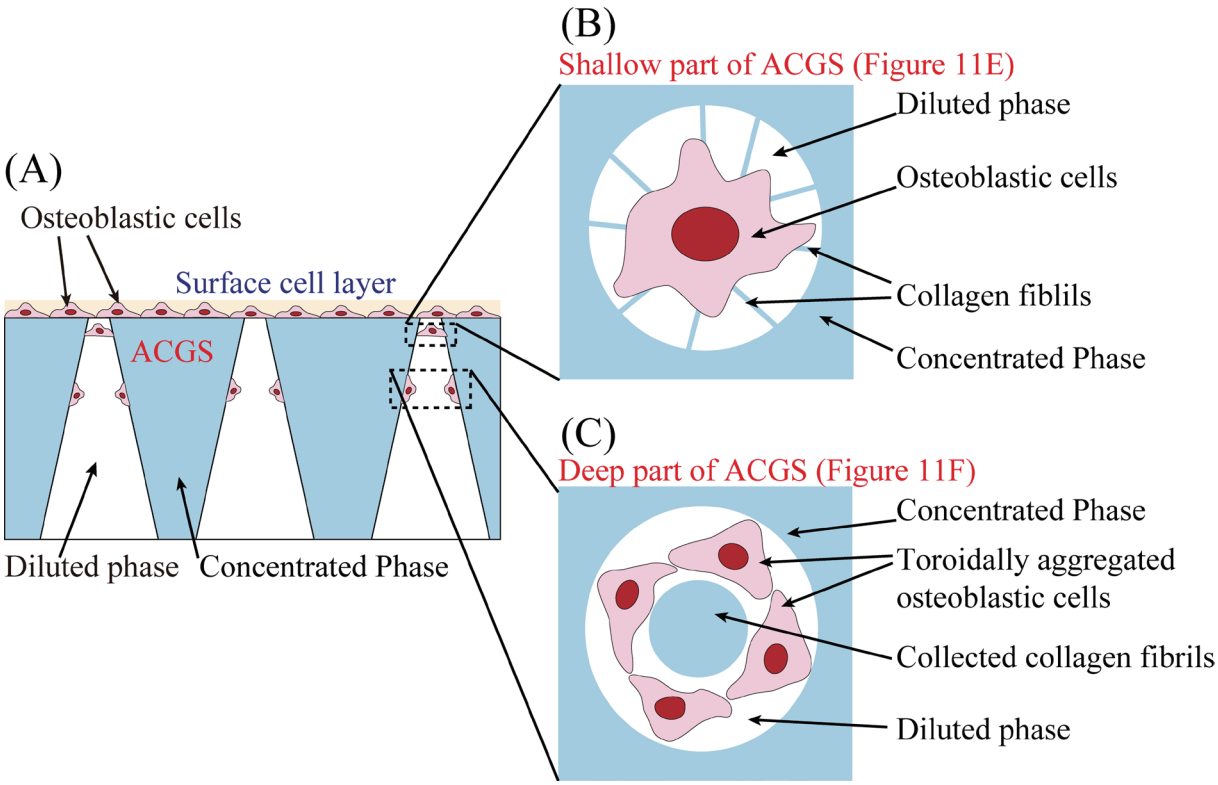


**Figure 12.** Schematic diagram of ACGS-osteoblasts composite.

(A) Cross-sectional view of ACGS-osteoblasts composite. At the ACGS surface, osteoblasts made a cell layer. Some cells invaded into the diluted phase. (B) Schematic diagram of Figure 11E. Osteoblast existed in the diluted phase, and looked pulling the bundle of the collagen fibrils from the interfacial wall between concentrated and diluted phases. (C) Schematic diagram of Figure 4F. Osteoblasts attach to the interface to construct a toroidally aggregating structure. In the center of the diluted phase, collagen fibrils that were presumably collected by osteoblasts existed.

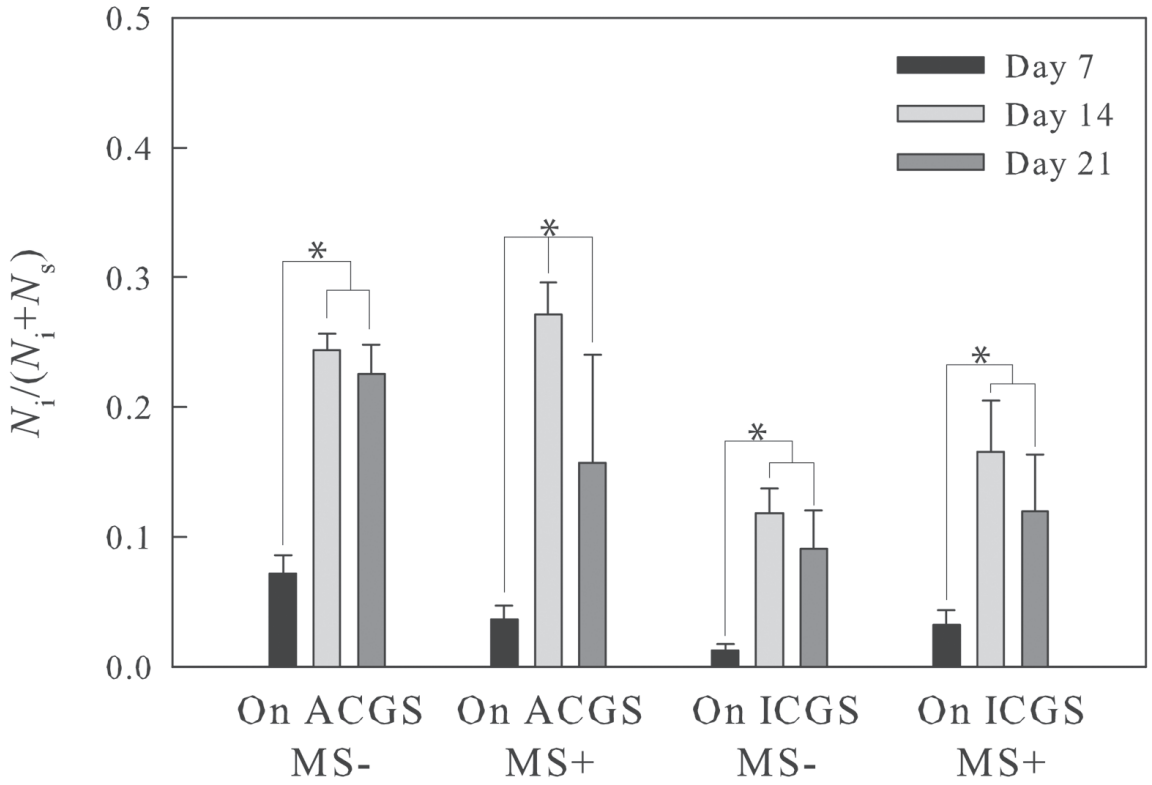


**Figure 13.** Quantification of cell numbers along with the time course of cell culture from 7 to 21 days.

The number of cells existing in the surface region is $N_s$, and that in the inner region is $N_i$. Specimens are ACGS-MS-, ACGS-MS+, ICGS-MS-, and IGCS-MS+. * indicate $p < 0.05$ significance.

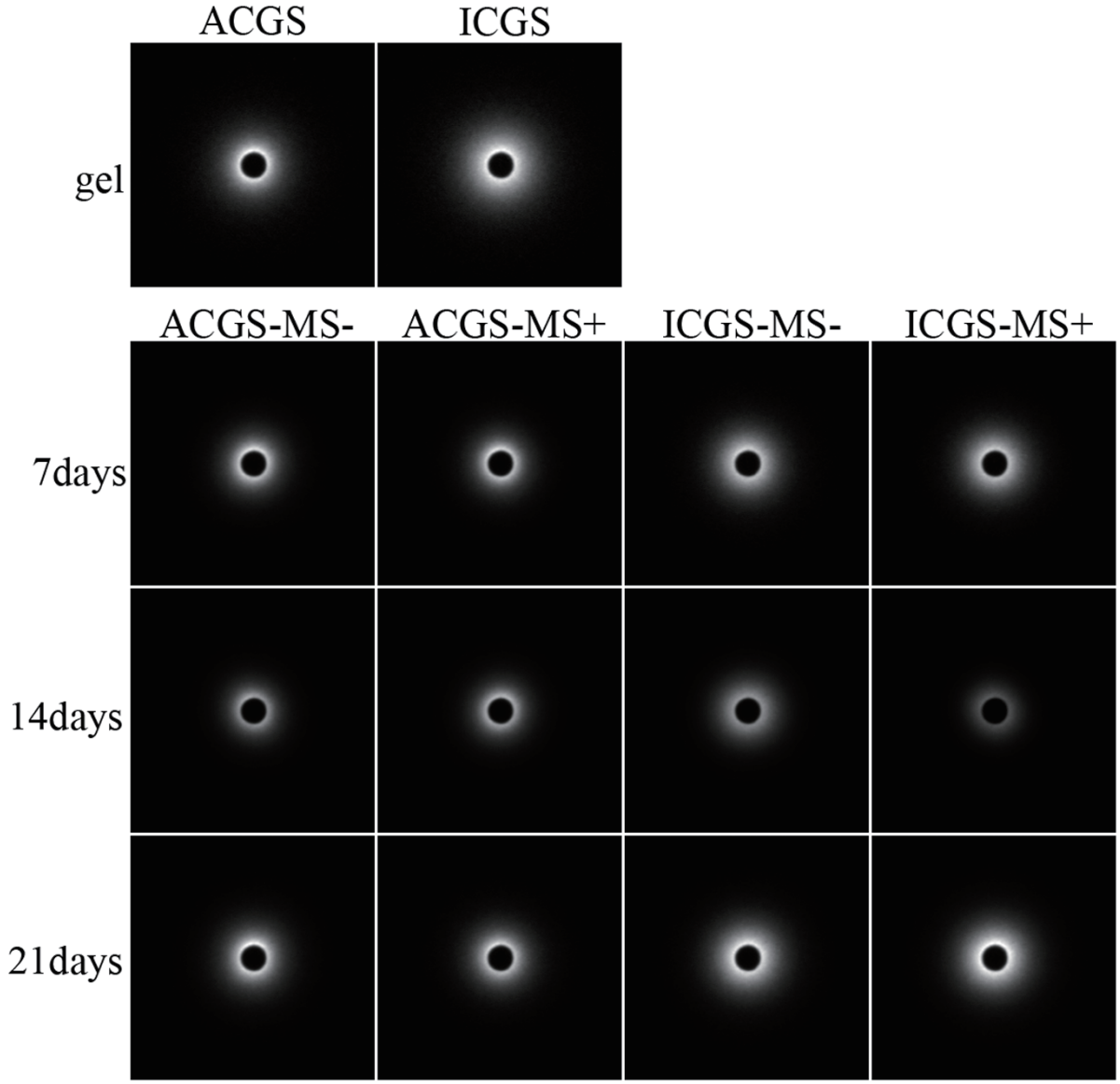


**Figure 14.** 2D SAXS patterns of SAXS profiles from scaffolds and cell-seeded specimens.

Specimens are ACGS, ICGS, ACGS-MS-, ACGS-MS+, ICGS-MS-, and ICGS-MS+. Cell-seeded specimens were cultured for 7 days, 14 days, and 21 days. Images show only the center region of each pattern.

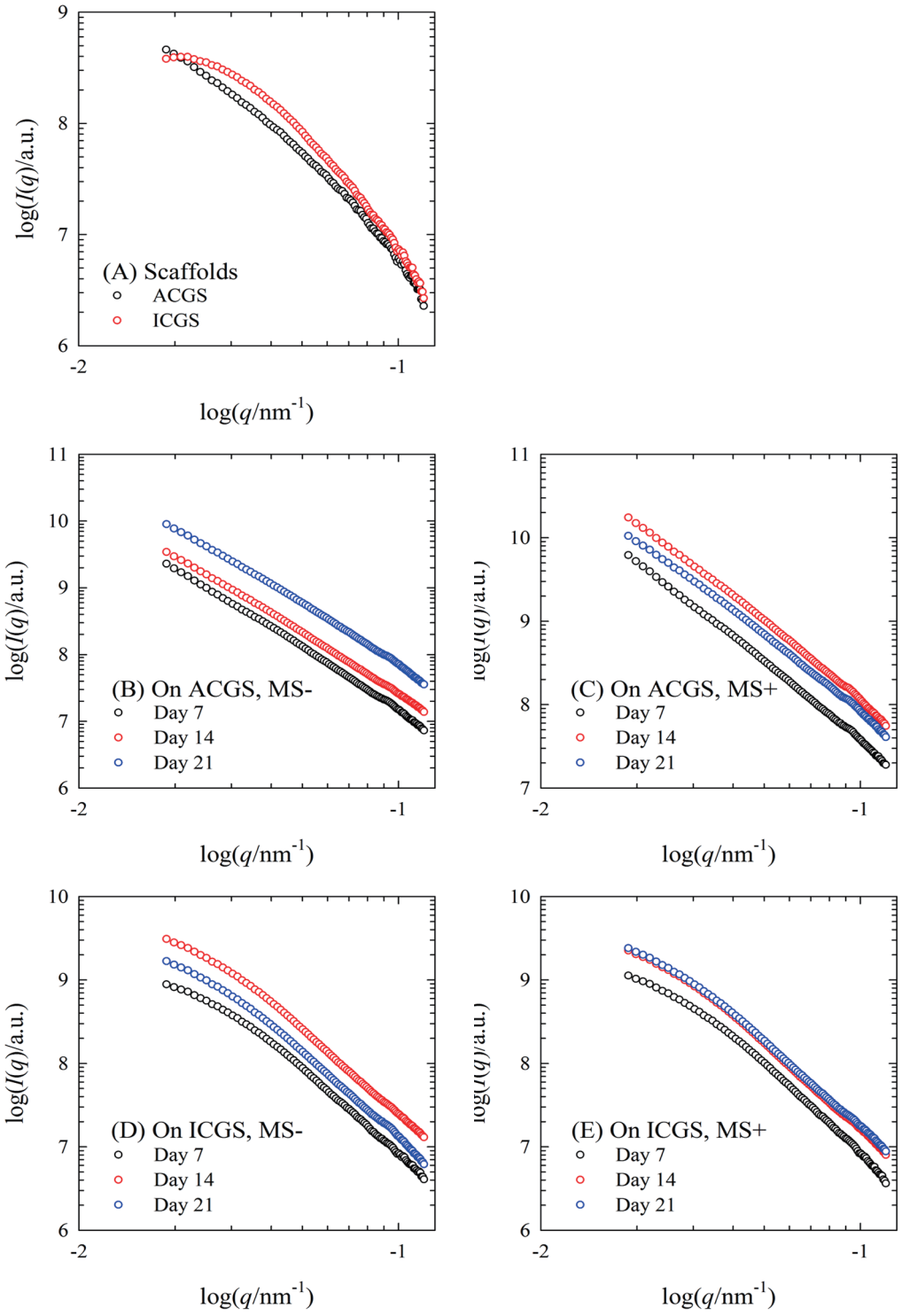


**Figure 15.** Log-log plots of SAXS profiles for scaffolds (A) and cell-seeded specimens (B)-(E).

Specimens are (A) ACGS and ICGS, (B) ACGS-MS-, (C) ACGS-MS+, (D) ICGS-MS-, and (E) ICGS-MS+. Cell-seeded specimens were cultured for 7 days, 14 days, and 21 days.

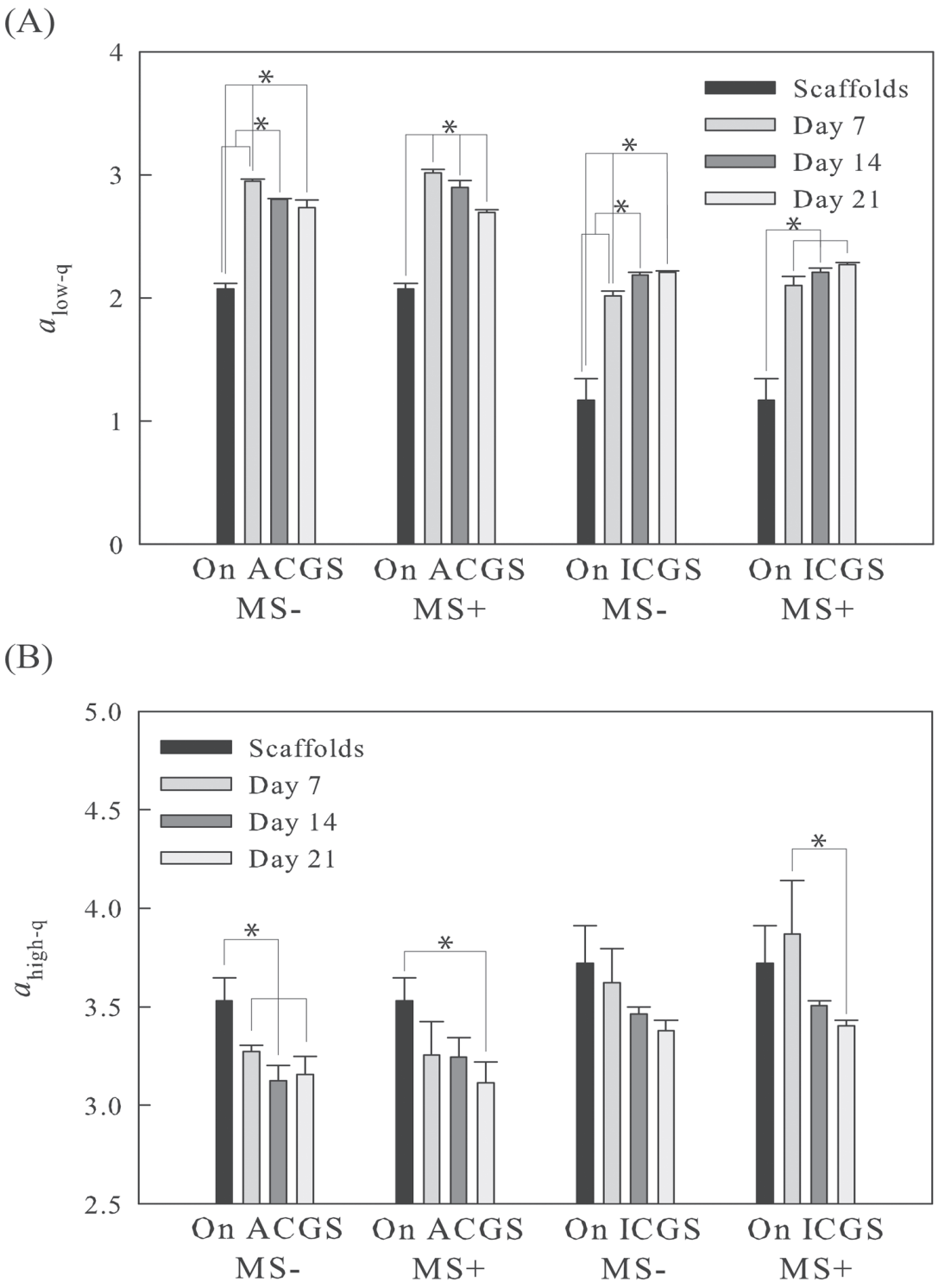


**Figure 16.** Scattering exponents determined from slopes of the straight lines in the low-q region (A) and high-q region (B) in log-log plots of SAXS profiles. Specimens are ACGS, ICGS, ACGS-MS-, ACGS-MS+, ICGS-MS-, and ICGS-MS+. Cell-seeded specimens were cultured for 7 days, 14 days, and 21days. * indicate $p < 0.05$ significance.

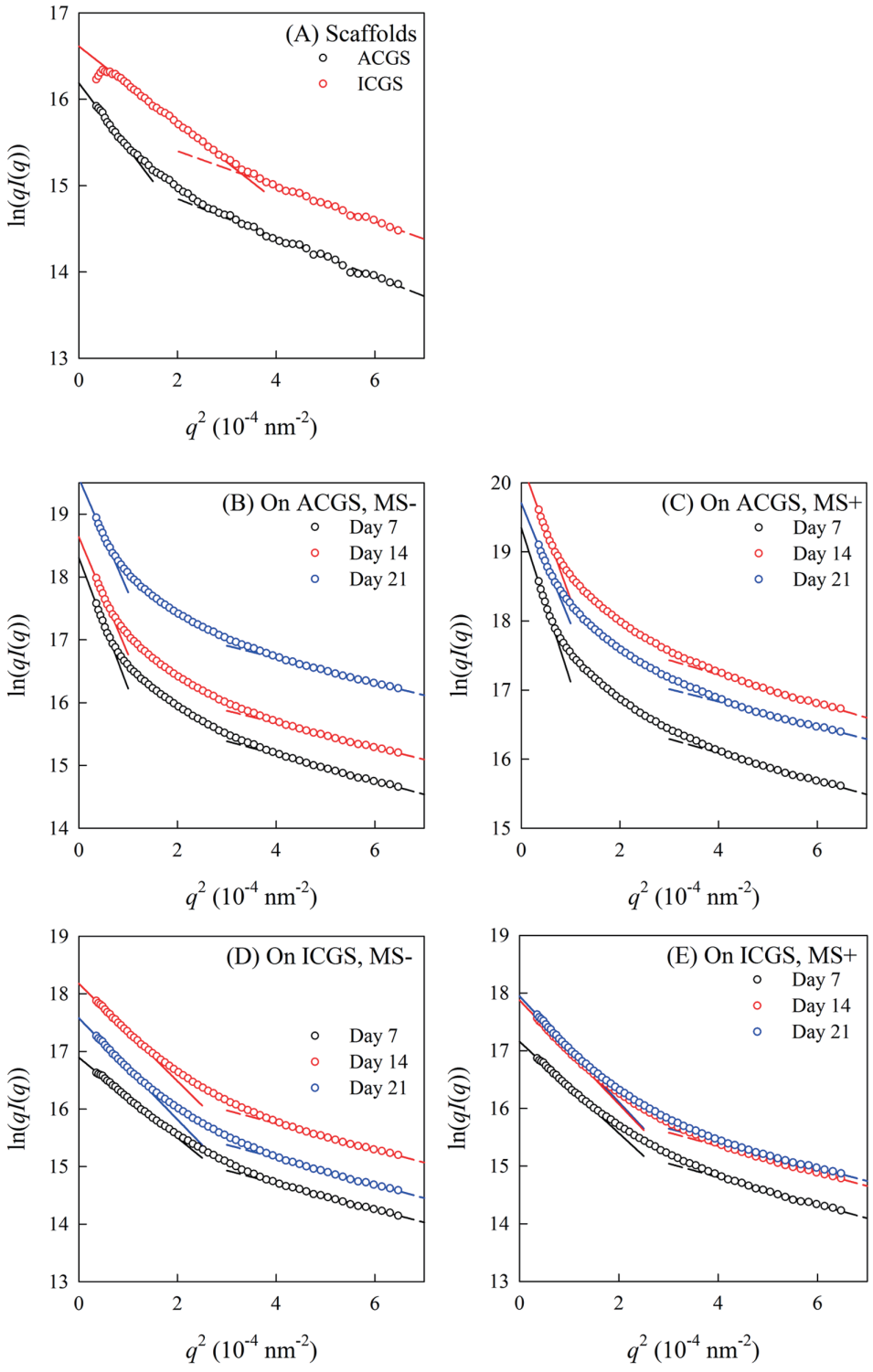


**Figure 17.** Cross-section Guinier plots of SAXS profiles for scaffolds (A) and cell-seeded specimens (B)-(E).

Specimens are (A) ACGS and ICGS, (B) ACGS-MS-, (C) ACGS-MS+, (D) ICGS-MS-, and (E) ICGS-MS+. Cell-seeded specimens were cultured for 7 days, 14 days, and 21 days.

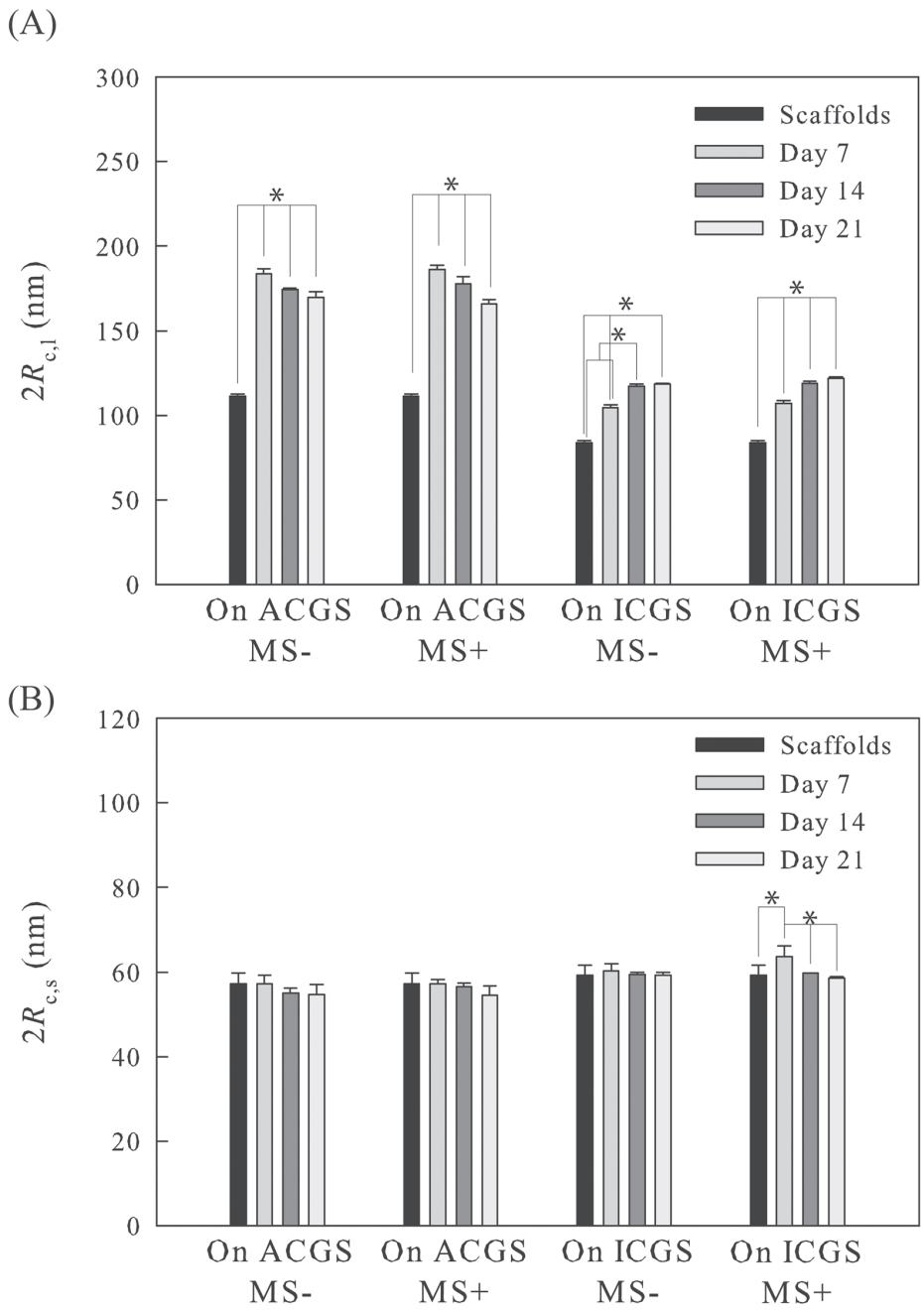


**Figure 18.** Diameters of the bundles of collagen fibrils (A) and a single collagen fibril (B) determined by the modified Guinier analysis.

Specimens are ACGS, ICGS, ACGS-MS-, ACGS-MS+, ICGS-MS-, and ICGS-MS+. Cell-seeded specimens were cultured for 7 days, 14 days, and 21 days.

$R_{c,l}$ was calculated by the radius of the cross-section for thick rod-like particles. $R_{c,s}$ was the radius of the cross-section for thin rod-like particles, which was calculated from the slope of the linear region observed in the high-q region of the cross-section Guinier plot.

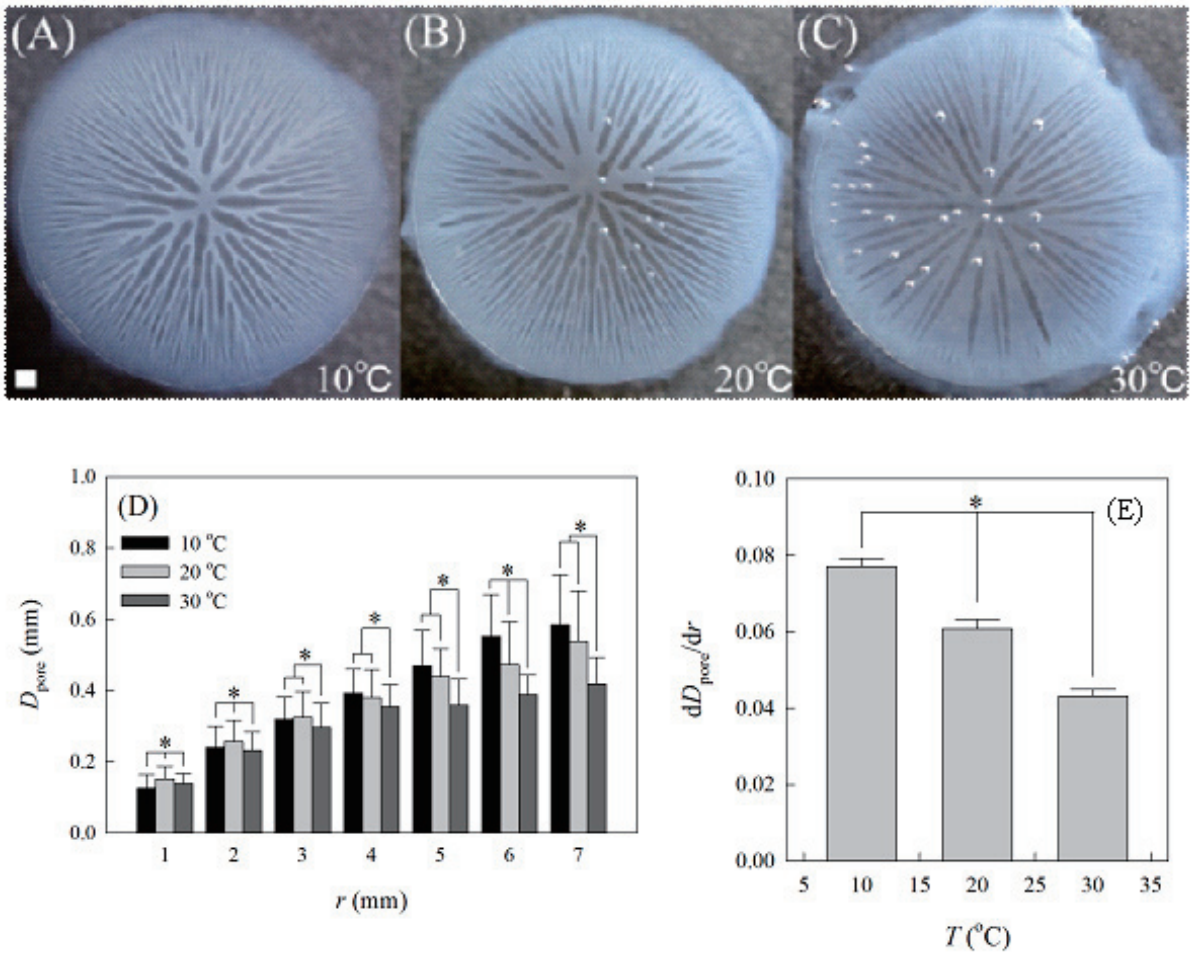


**Figure 19**. Effect of temperature on macroscopic structure of ACGS. Opcical photographs of the ACGS films fabricated at 10 ℃ (A), 20 ℃ (B), and 30 ℃ (C). Scale bar = 1 mm. (D): Positional ($r$) dependences of diameters of diluted phase ($D_{pore}$). (E): Temperature dependence of slopes calculated from the plots of $D_{pore}$ vs. $r$, ($dD_{pore}/dr$). * indicates $p < 0.05$ significance.

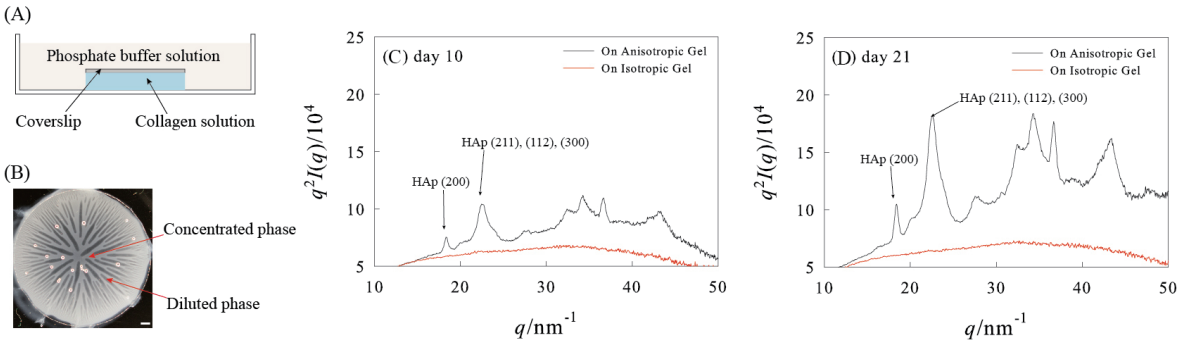


**Figure 20**. Wide-angle X-ray diffraction (WAXD) analysis of the anisotropic and isotropic collagen gel with osteoblast cultivation.

(A) Schematic diagram of the anisotropic collagen gel formation. (B) Optical image of the anisotropic collagen gel. Tube-like diluted phase radially extended from the center of the gel. Scale bar = 1 mm. 1D WAXD profile of osteoblastic cell-gel composite film cultured until day 10 (C) and 21 (D) on the anisotropic and isotropic collagen gel for control. Incident X-ray beam was perpendicular to the film.

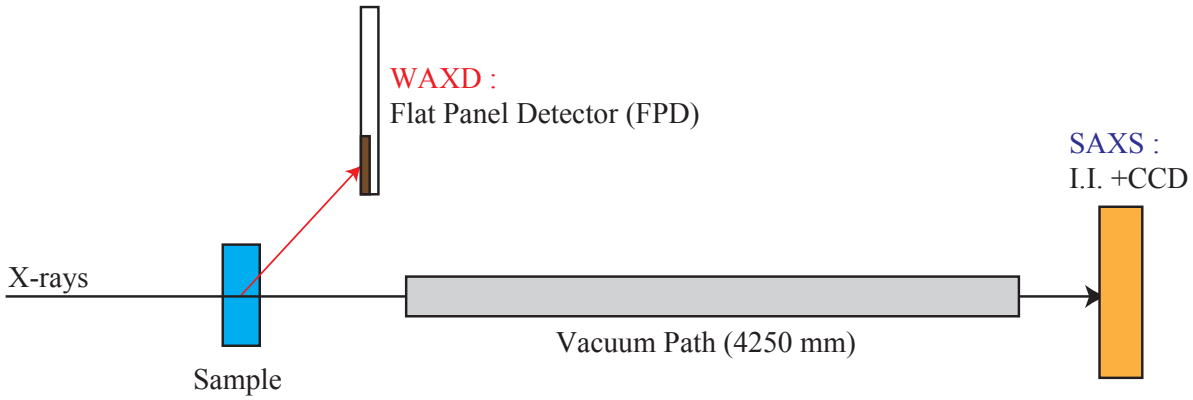


**Figure 21**. Scheme of optical system for simultaneous measurement of SAXS and WAXD in SPring-8 BL40B2 beamline.

SAXS patterns were acquired with a CCD with an X-ray imaging intensifier (I. I.), and sample-to-detector distance was 4250 mm. WAXD pattern was obtained by flat panel detector between vacuum path and sample.

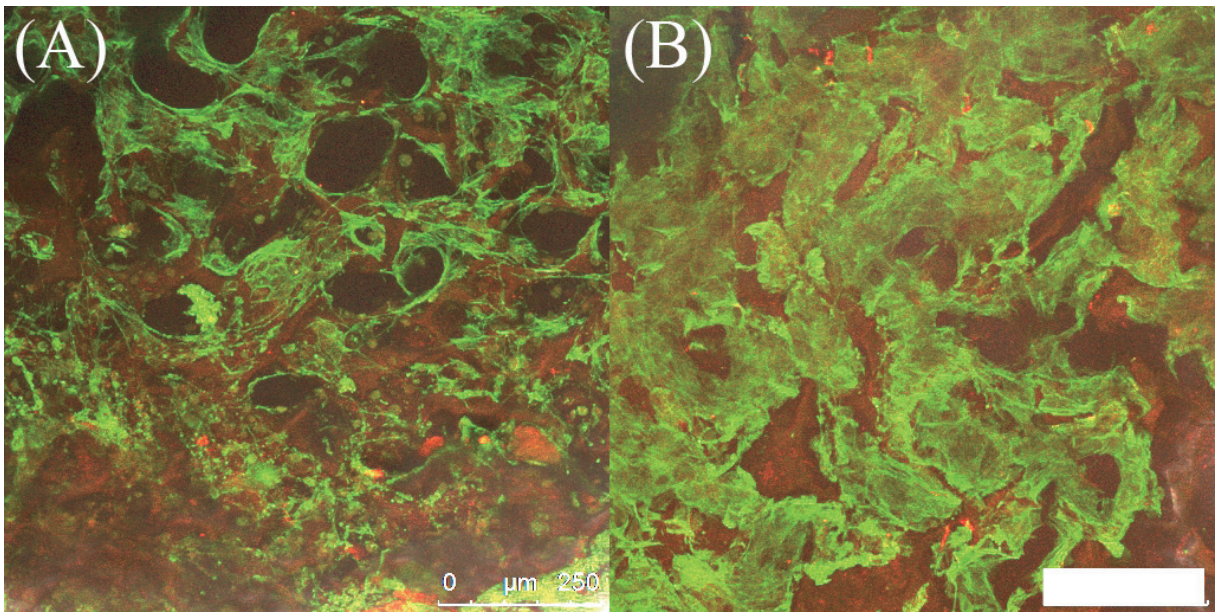


**Figure 22**. Cell attachment assay

Actin fiber (green) and collagen (red) were visualized in MS+ (A) and MS- (B) specimens. Cultivation time is 7 days. Scale bar = 250 $\mu$ m.

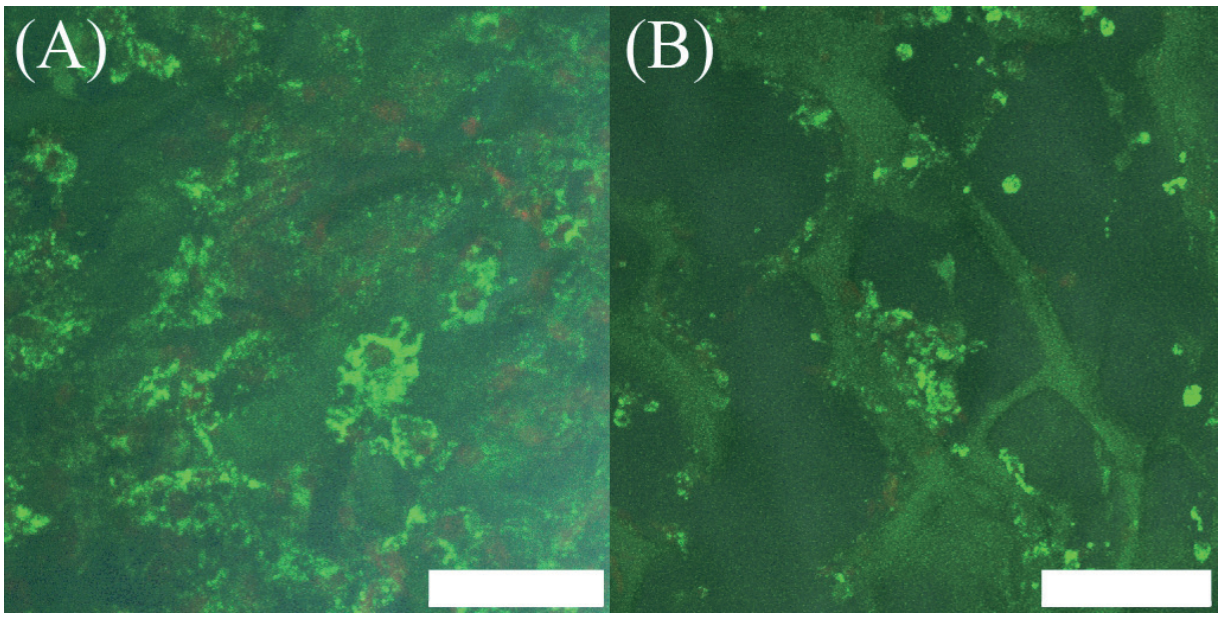


**Figure 23**. Cell viability assay

Live cells (green) and dead cells (red) were visualized in MS+ (A) and MS- (B) specimens. Cultivation time is 14 days. Scale bar = (A) 75 $\mu$ m and (B) 200 $\mu$ m.

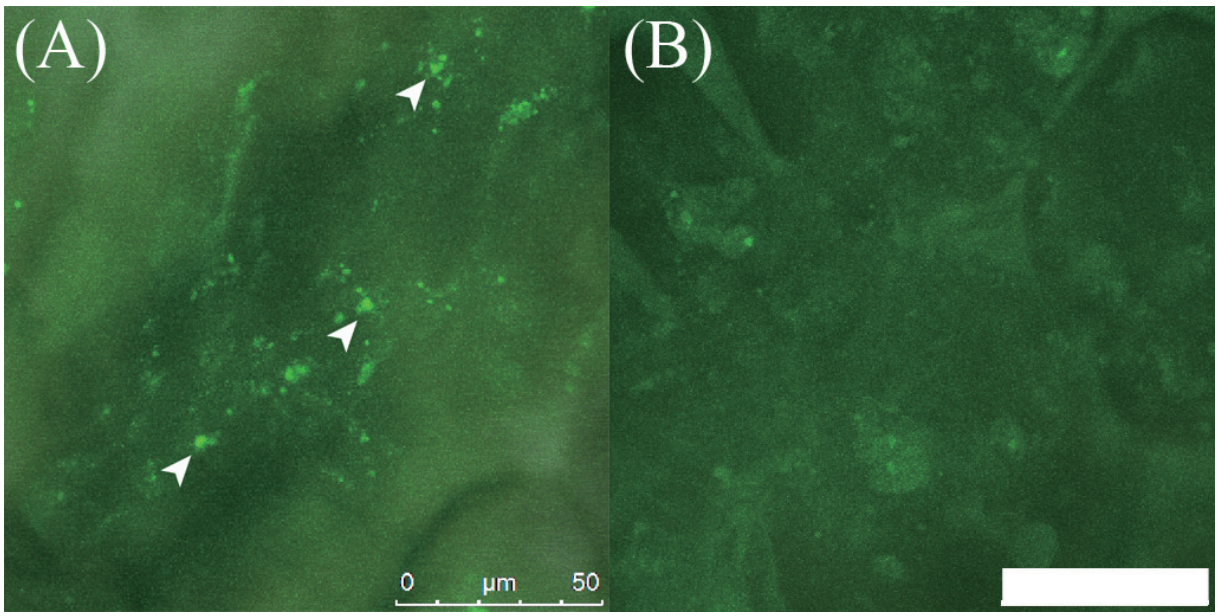


**Figure 24**. Calcium staining at 21 days cultivation.

Calcium ions (green) were visualized in MS+ (A) and MS- (B) specimens. In MS applied specimens, spheroidal calcium particles (arrow head) were observed. Scale bar = 50 $\mu$ m.

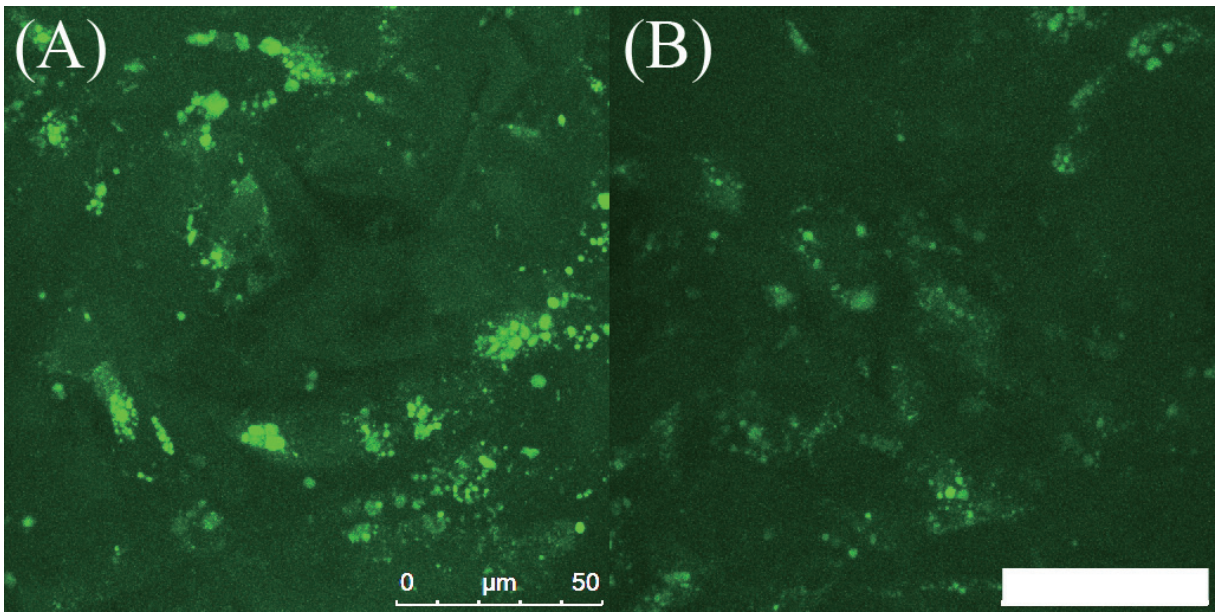


**Figure 25**. Calcium staining at 28 days cultivation.

Calcium ions (green) were visualized in MS+ (A) and MS- (B) specimens. Spheroidal calcium particles were observed in both specimens, but fluorescent intensity of MS+ specimen is much higher than that of MS-.observed. Scale bar = 50 $\mu$ m.

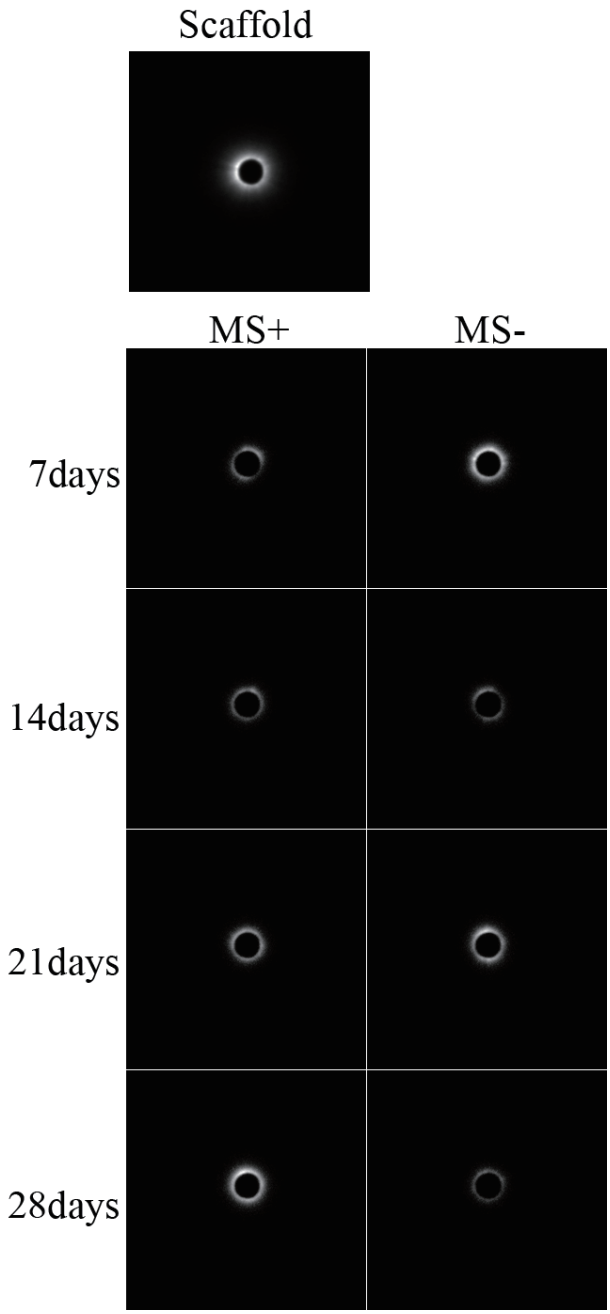


**Figure 26.** 2D SAXS patterns of cell-seeded collagen sponges.

Specimens are Scaffold, MS- and MS+. Cell-seeded specimens were cultured for 7 days, 14 days, 21 days, and 28 days. Images show only the center region of each pattern.

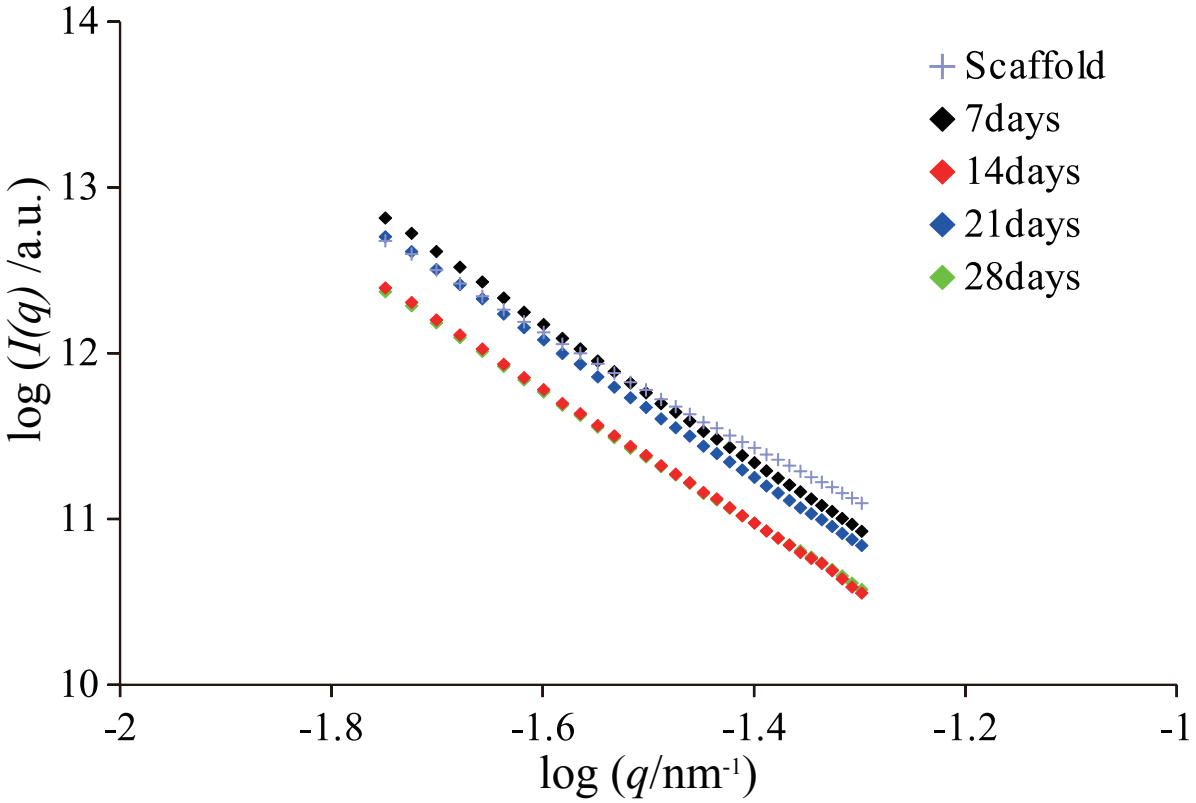


**Figure 27.** 1D SAXS profiles of cell-seeded collagen sponges.

Specimens are Scaffold and MS-. Cell-seeded specimens were cultured for 7 days, 14 days, 21 days, and 28 days.

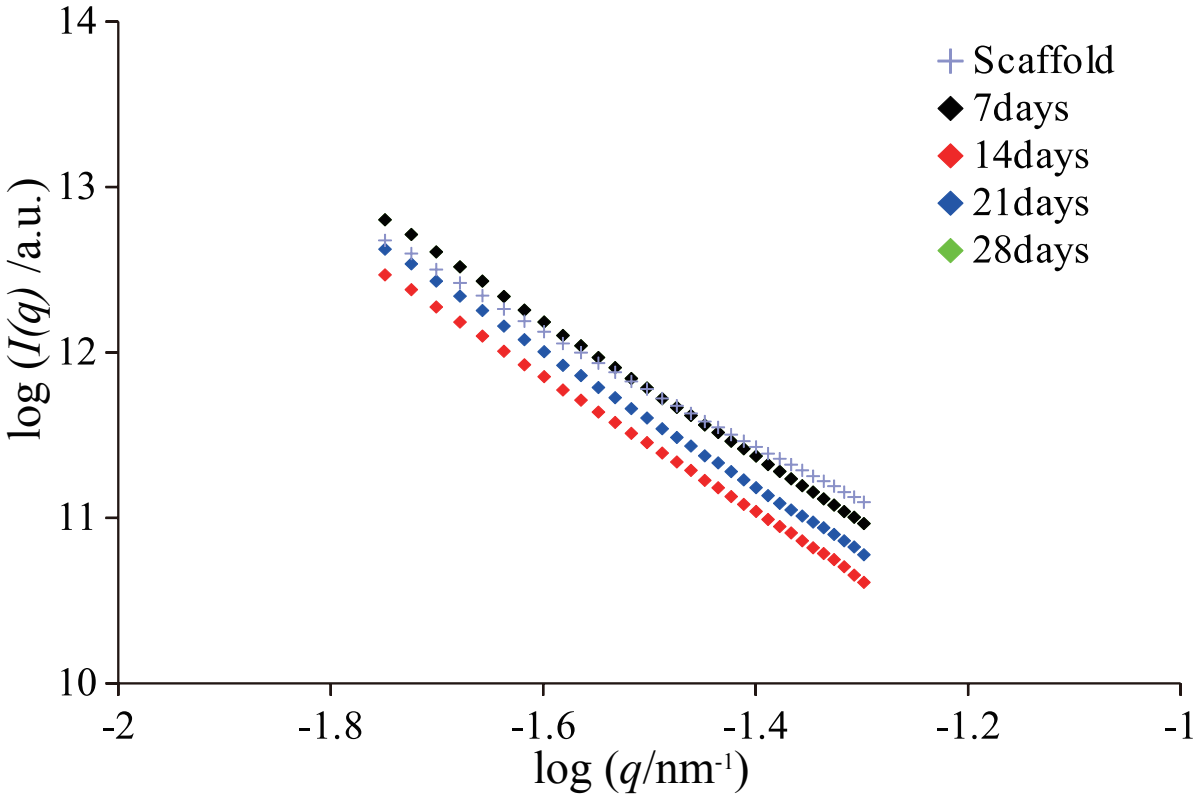


**Figure 28.** 1D SAXS profiles of cell-seeded collagen sponges.

Specimens are Scaffold and MS+. Cell-seeded specimens were cultured for 7 days, 14 days, 21 days, and 28 days.

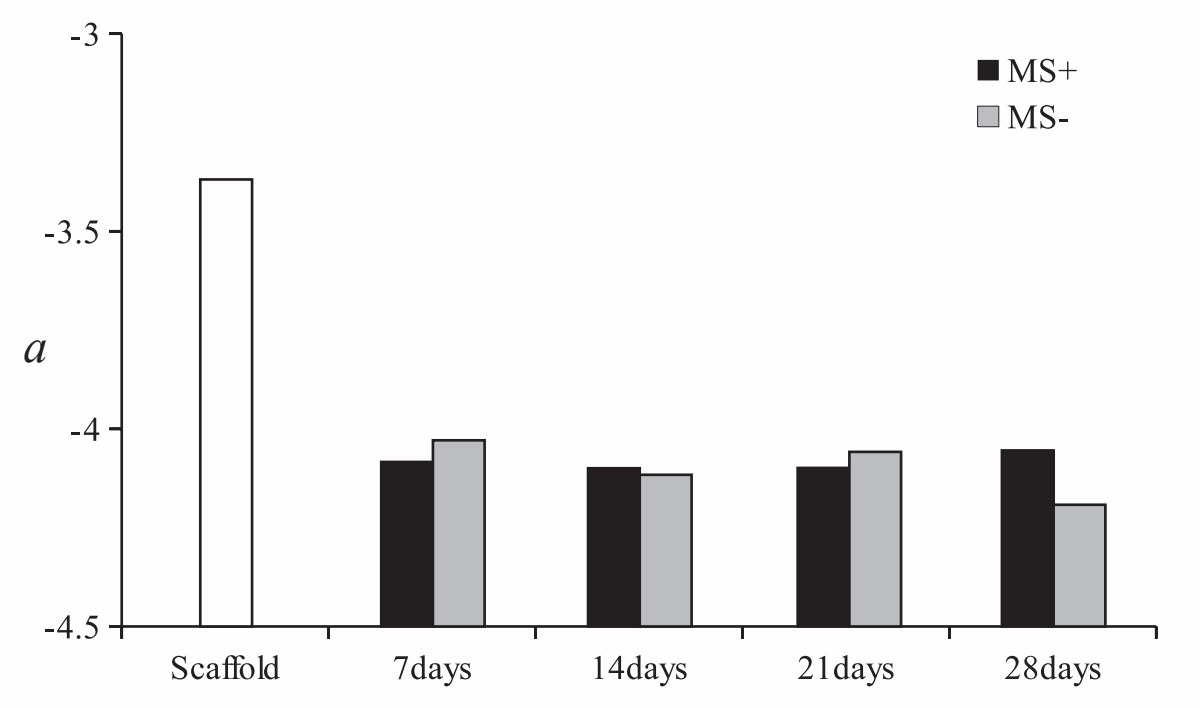


**Figure 29.** Scattering exponents determined from slopes in log-log plots of SAXS profiles.

Specimens are Scaffold, MS- and MS+. Specimens were cultured for 7 days, 14 days, 21 days and 28 days.

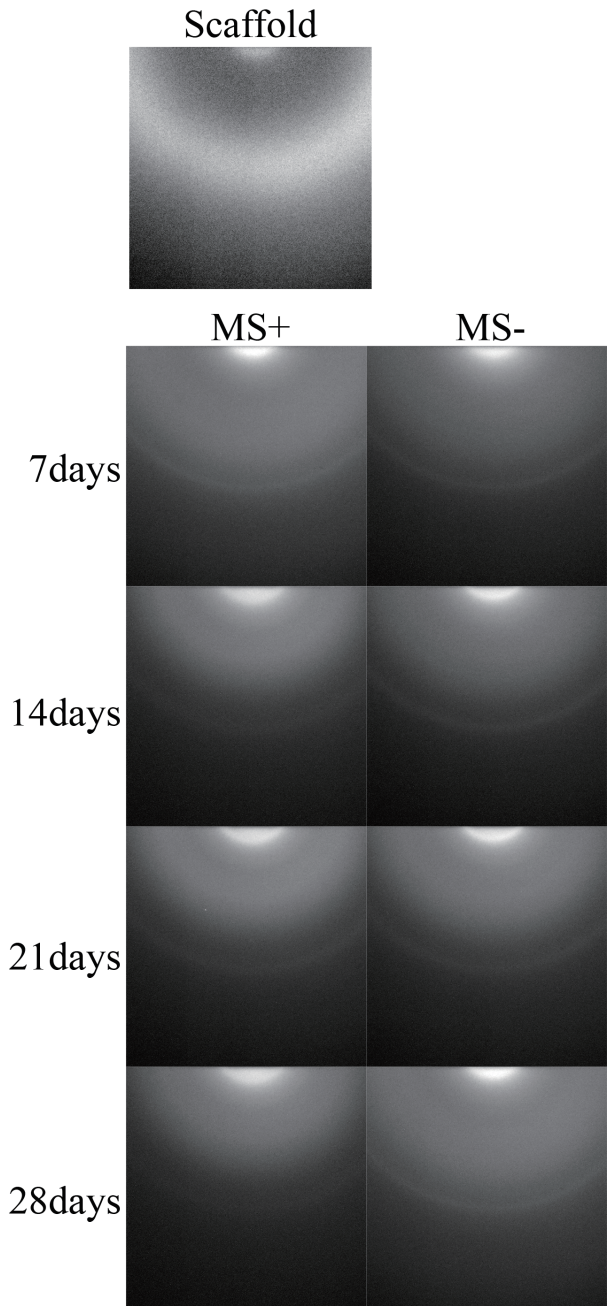


**Figure 30.** 2D WAXD patterns of cell-seeded collagen sponges.

Specimens are Scaffold, MS- and MS+. Cell-seeded specimens were cultured for 7 days, 14 days, 21 days, and 28 days. Images show only the center region of each pattern.

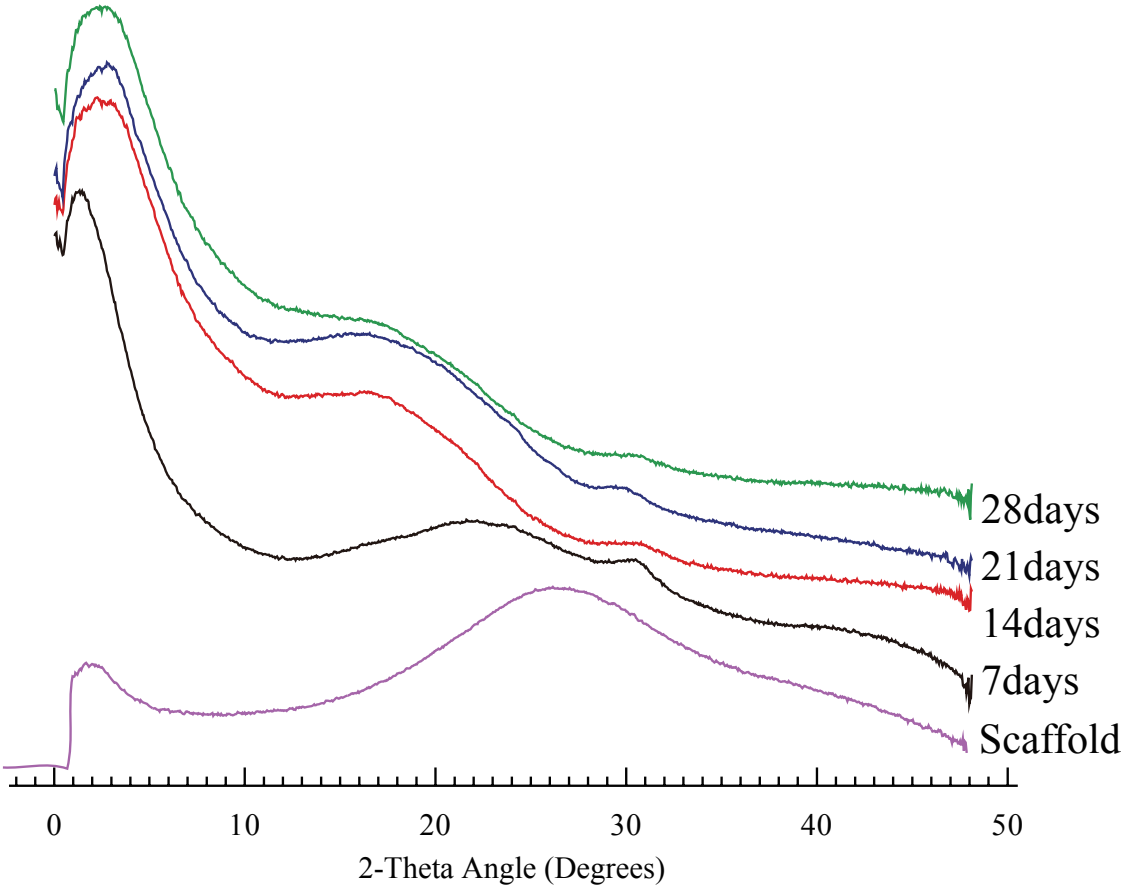


**Figure 31.** 1D WAXD profiles of cell-seeded collagen sponges.

Specimens are MS+. Cell-seeded specimens were cultured for 7 days, 14 days, 21 days, and 28 days.

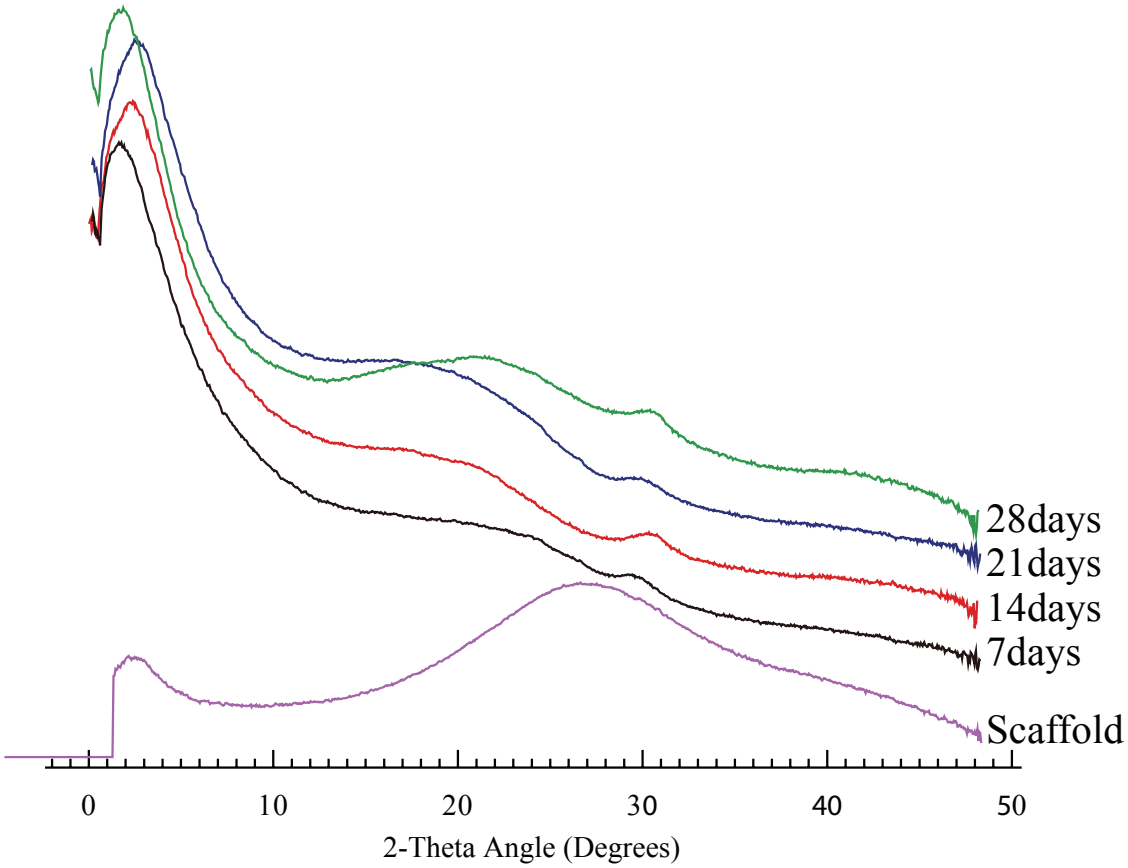


**Figure 32.** 1D WAXD profiles of cell-seeded collagen sponges.

Specimens are MS-. Cell-seeded specimens were cultured for 7 days, 14 days, 21 days, and 28 days.